

Real-space quantum-to-classical transition of time dependent background fluctuations

S. Mahesh Chandran,^{1,*} Karthik Rajeev,^{1,†} and S. Shankaranarayanan^{1,‡}

¹*Department of Physics, Indian Institute of Technology Bombay, Mumbai 400076, India*

Abstract

Understanding the emergence of classical behavior from a quantum theory is vital to establishing the quantum origin for the temperature fluctuations observed in the Cosmic Microwave Background (CMB). We show that a real-space approach can comprehensively address the quantum-to-classical transition problem in the leading order of curvature perturbations. To this end, we test spatial bipartitions of quadratic systems for the interplay between three different signatures of classical behavior — i) decoherence, ii) peaking of the Wigner function about classical trajectories, and iii) relative suppression of non-commutativity in observables. We extract these signatures from the covariance matrix of a multi-mode Gaussian state and address them primarily in terms of entanglement entropy and log-classicality. Through a phase-space stability analysis of spatial sub-regions via their reduced Wigner function, we ascertain that the underlying cause for the dominance of classicality signatures is the occurrence of gapped inverted mode instabilities. While the choice of conjugate variables enhances some of these signatures, decoherence studied via entanglement entropy is the stronger and more reliable condition for classicality to emerge. We demonstrate the absence of decoherence, which preempts a quantum-to-classical transition of scalar fluctuations in an expanding background in $(1+1)$ -dimensions using two examples — i) a Tanh-like expansion and ii) a de-Sitter expansion. We then extend the analysis to leading order fluctuations in $(3+1)$ -dimensions to show that a quantum-to-classical transition occurs in the de-Sitter expansion and discuss the relevance of our analysis in distinguishing cosmological models.

* maheshchandran@iitb.ac.in

† karthik_rajeev@iitb.ac.in

‡ shanki@iitb.ac.in

I. INTRODUCTION

The emergence of the Universe’s classical behavior from its predominantly quantum mechanical early stage is one of the most intriguing phenomena in cosmology [1, 2]. This fascinating process is believed to be rooted in the dynamics shared by generic quantum systems when they interact with their environments. A crucial effect in this context is the loss of quantum coherence induced by the environment. Quantum coherence is a fundamental property of quantum mechanics that results from the superposition of orthogonal states with regard to a reference basis [3]. Specifically, it refers to the ability of a quantum system to maintain a well-defined quantum state over time, unaffected by external disturbances or interactions. Quantum coherence is necessary for both entanglement [4] and other measures of quantum correlations (like discord, negativity, and circuit complexity). It is also vital for quantum computing because quantum algorithms depend on the ability to manipulate and preserve superposition and entanglement.

Due to the nature of closed quantum evolution, quantum coherence can never vanish permanently from a closed quantum system. However, realistic physical systems are embedded in an inaccessible or partially accessible environment. A quantum system will typically become entangled with many environmental degrees of freedom when interacting with the environment. This entanglement can in turn non-trivially affect local measurements made in the system. Quantum systems progressively lose coherence to the environment due to interactions with the external environment and can be treated as classical [5, 6]. As a closed system, the origin of the classical world requires explanation.

Returning to the cosmological scenario, the Cosmic Microwave Background (CMB) [7, 8] provides essential proof of temperature variations in a relatively homogeneous distribution of matter, radiation, and (potentially) dark energy. These inhomogeneities can be traced all the way back to the early-Universe, and are understood to be seeded by vacuum quantum fluctuations stretched to cosmological scales during a rapidly expanding *inflationary* phase [9–13]. Interestingly, such inhomogeneities, when treated as classical stochastic fluctuations seeded in the CMB after the end of inflation, provide a compelling explanation for the evolution of large-scale structures in the Universe as observed at late-times [14–18]. Then the questions of how vacuum fluctuations evolved to resemble classical fluctuations, and how non-trivial signatures of such a transition can be observed, become pertinent towards establishing the

quantum origin of CMB fluctuations [19–22].

While there is no single, unified criterion for the emergence of classicality within a quantum field theoretical framework, it is largely addressed via a collection of phenomenological signatures associated with different facets of classical behavior. For instance, as a result of the mixing of the super-Hubble (system) and sub-Hubble (environment) momentum-modes of fluctuations due to non-linear curvature perturbations, the super-Hubble modes are found to *decohere*. A continuously evolving quantum information toolbox comprising of quantum entanglement [23–26], quantum discord [18, 27, 28], open-effective field theory (EFT) approaches [29, 30], in the momentum space has lately proved decisive in making robust predictions for the (extremely rapid) decoherence rate and the (highly suppressed) quantum corrections to the power spectrum resulting from this. However, these signatures are reportedly too small to be captured by current observations. Furthermore, the absence of decoherence in the leading (linear) order of curvature perturbations due to mode-decoupling, and various pitfalls associated with the emergence of classical behaviour in squeezed quantum states have been critically addressed in recent works [31–33].

A real-space approach towards understanding quantum-classical transition is much less explored in this context, in spite of providing a more intuitive picture of field entanglement [4, 34–38] and its underlying connection with the thermodynamic properties of the background space-time [39–42]. While this may have much to do with real-space field-entanglement being plagued by UV-divergences, recent works have proposed ways in which the sensitivity to UV-cutoff can be mitigated through field-smearing in disjoint spatial regions [33, 43, 44] or scaling symmetry arguments [45]. However, as we will show in this work, the biggest advantage of the real-space picture is that it captures phenomenological signatures of quantum-classical transition even up to the linear order of curvature perturbations. Therefore, the resulting quantum corrections are expected to be significantly less suppressed than in the momentum-space picture.

To identify quantum-classical transition in the real space, we test spatial bipartitions of leading order fluctuations for three different signatures of classical behavior — i) loss of quantum coherence, which allows the system to be well described by a classical statistical ensemble, ii) peaking of the phase-space distribution of the quantum state about classical trajectories, and iii) relative suppression of non-commutativity. While these signatures may jointly manifest in the momentum-space picture for (higher-order) fluctuations propagating

in a (near) de-Sitter background, they are in general inequivalent for the broader class of quantum systems [22]. Therefore, the exact interplay between these concepts in real space will be relevant not only for early-Universe fluctuations but also for any quantum system with entangled spatial degrees of freedom. In turn, its applications potentially extend to laboratory simulators for time-dependent backgrounds [46–48] as well as table-top experiments being proposed for detecting “quantumness” of gravity in the coming years [49–52].

The paper is organized as follows: In Section II, we develop the tools to extract and measure the aforementioned signatures of classicality in time-dependent quadratic systems, in particular, the CHO system, in detail. Through a phase-space stability analysis of Gaussian states, we identify the presence of gapped inverted modes (in the momentum space) of the entire system as the primary trigger for the quantum-to-classical transition of subsystems (in the real space). In Section III, we study the effects of canonical transformations on classicality criteria. In Section IV, we demonstrate the absence of quantum-to-classical transition of scalar fluctuations in an expanding background in $(1+1)$ –dimensions using two examples — i) a Tanh-like expansion and ii) a de-Sitter expansion. Section V extends the analysis to $(3+1)$ –dimensions to show that the quantum-to-classical transition occurs in the de-Sitter expansion but not in the Tanh-expansion. In Section VI, we discuss the physical interpretation of our results and future directions. Throughout this work, we use metric signature $(+, -, -, -)$ and set $\hbar = c = 1$ unless otherwise specified.

II. QUANTUM-TO-CLASSICAL TRANSITION IN TIME-DEPENDENT OSCILLATORS

In this section, we analyse the signatures of quantum-classical transition in the phase-space representation of quantum states. We begin our analysis with the coupled harmonic oscillator (CHO) system, which serves as a fundamental building block for the lattice-regularized approach to field theory that will be extensively studied in the later sections. The Hamiltonian for such a system is characterized by a frequency $\omega(t)$ and a coupling parameter $\chi(t)$, both of which are arbitrary (smooth, bounded) functions of time:

$$\mathcal{H}(t) = \frac{p_1^2}{2} + \frac{p_2^2}{2} + \frac{1}{2}\omega^2(t)(x_1^2 + x_2^2) + \frac{1}{2}\chi^2(t)(x_1 - x_2)^2 \quad (1)$$

Under the transformations $x_{\pm} = (x_1 \pm x_2)/\sqrt{2}$, the above Hamiltonian reduces to:

$$\mathcal{H}(t) = \frac{p_+^2}{2} + \frac{p_-^2}{2} + \frac{1}{2}\omega_+^2(t)x_+^2 + \frac{1}{2}\omega_-^2(t)x_-^2, \quad (2)$$

where the time-dependent normal modes are:

$$\omega_-(t) = \sqrt{\omega^2(t) + 2\chi^2(t)}; \quad \omega_+(t) = \omega(t). \quad (3)$$

We consider the form-invariant Gaussian state (GS), which takes the form [53]:

$$\Psi_{\text{GS}}(x_+, x_-, t) = \prod_{j=\{+,-\}} \left(\frac{\omega_j(t_0)}{\pi b_j^2(t)} \right)^{1/4} \exp \left\{ - \left(\frac{\omega_j(t_0)}{b_j^2(t)} - i \frac{\dot{b}_j(t)}{b_j(t)} \right) \frac{x_j^2}{2} - \frac{i}{2} \omega_j(t_0) \tau_j(t) \right\}, \quad (4)$$

where $\tau_j = \int b_j^{-2}(t) dt$. The scaling parameters b_j are solutions of the non-linear Ermakov-Pinney equation [53–56] :

$$\ddot{b}_j(t) + \omega_j^2(t) b_j(t) = \frac{\omega_j^2(t_0)}{b_j^3(t)} \quad (5)$$

The scaling parameters $b_j(t)$ drive the evolution of the Gaussian state as well as its deviation from the initial vacuum state defined at $t = t_0$. While the system evolves to an excited state in the corresponding instantaneous eigenbasis at later time-slices [57, 58], its state remains pure [$\text{Tr } \rho^2 = 1$] over the course of the evolution. The dynamics of the constituent subsystems (x_1, x_2) , on the other hand, may exhibit interesting properties by virtue of the entanglement between them. Notably, one subsystem may act as an external environment to the other, causing the latter to “decohere”, or lose some of its quantum features. To illustrate this in the case of CHO, we describe one constituent oscillator (say, x_2) with the help of its reduced density matrix (RDM), obtained by tracing out the other oscillator (viz., x_1) from the full density matrix of the CHO:

$$\begin{aligned} \rho_2(x_2, x'_2) &= \int dx_1 \Psi_{\text{GS}}^*(x_1, x'_2) \Psi_{\text{GS}}(x_1, x_2) \\ &= \left(\frac{K_+ K_-}{2\pi \text{Re}(A)} \right)^{1/2} \exp \left\{ - \frac{\Gamma_1}{2} (x_2^2 + x_2'^2) + \Gamma_2 x_2 x_2' + i \frac{\Gamma_3}{2} (x_2^2 - x_2'^2) \right\}, \end{aligned} \quad (6)$$

where

$$\begin{aligned}
\Gamma_1 &= 2A_R - \left(\frac{B_R^2 - B_I^2}{A_R} \right) \quad ; \quad \Gamma_2 = \frac{|B|^2}{A_R} \quad ; \quad \Gamma_3 = 2A_I - \frac{2B_R B_I}{A_R} \\
A &= \frac{1}{4} [(K_+ + K_-) - i(L_+ + L_-)] = A_R + iA_I \\
B &= \frac{1}{4} [-(K_+ - K_-) + i(L_+ - L_-)] = B_R + iB_I \\
K_{\pm} &= \frac{\omega_{\pm}(t_0)}{b_{\pm}^2(t)} \quad ; \quad L_{\pm} = \frac{\dot{b}_{\pm}(t)}{b_{\pm}(t)}
\end{aligned} \tag{7}$$

To identify possible signatures of a quantum-classical transition, it is useful to shift to a phase-space representation of the above reduced density matrix.

A. Classicality criteria from phase-space representation

A phase-space picture is possible within the framework of quantum mechanics with the help of Wigner-Weyl transform [59–61], which maps operators to phase-space functions:

$$\mathcal{W}[\hat{O}] \rightarrow O(x, p). \tag{8}$$

The Wigner-Weyl transform of the density matrix $\rho(x, x')$, also known as the Wigner function, therefore provides a phase-space distribution pertaining to a quantum state:

$$W(x_c, p) = \mathcal{W}[\hat{\rho}] = \frac{1}{2\pi} \int_{-\infty}^{\infty} dx_{\Delta} \rho \left(x_c - \frac{x_{\Delta}}{2}, x_c + \frac{x_{\Delta}}{2} \right) e^{-ipx_{\Delta}}, \tag{9}$$

where

$$x_c = \frac{x + x'}{2} \quad ; \quad x_{\Delta} = x - x'. \tag{10}$$

For Gaussian states, the Wigner function takes the following form [57, 62]:

$$W(x, p) = \frac{\alpha}{2\pi\gamma} \exp \left\{ -\frac{(p - \beta x)^2}{4\gamma^2} - \alpha^2 x^2 \right\}. \tag{11}$$

In particular, the parameters characterizing the (reduced) Wigner function for the reduced density matrix given in (6), which shall be our focus in this section, are equated below:

$$\alpha^2 = \Gamma_1 - \Gamma_2 \quad ; \quad \gamma^2 = \frac{\Gamma_1 + \Gamma_2}{4} \quad ; \quad \beta = \Gamma_3, \tag{12}$$

where Γ_1, Γ_2 and Γ_3 are as defined in (7).

The Wigner function is a distribution in the phase-space that exactly captures the probabilistic nature and non-trivial effects (e.g., interference, entanglement) of quantum states in

a system, in contrast to well-defined trajectories pertaining to its classical counterpart. The expectation values for observables can be calculated using averages weighted by the Wigner distribution:

$$\langle \hat{O} \rangle = \int dx \int dp W(x, p, t) \mathcal{W}[\hat{O}] \quad (13)$$

For Gaussian states, the following averages (two-point correlators), computed in the above manner, encode all information about the system:

$$\langle \{\hat{x}, \hat{x}\} \rangle = \frac{1}{\alpha^2} \quad ; \quad \langle \{\hat{p}, \hat{p}\} \rangle = \frac{\beta^2}{\alpha^2} + 4\gamma^2 \quad ; \quad \langle \{\hat{x}, \hat{p}\} \rangle = \frac{\beta}{\alpha^2} \quad (14)$$

To better visualize the phase-space features of a Gaussian state, it is convenient to introduce the dimensionless quadratures $P = \frac{p}{\sqrt{2\alpha\gamma}}$ and $X = \sqrt{2\alpha\gamma}x$, in terms of which the Wigner function takes the general form:

$$W(X, P) = \frac{\delta_{QD}}{\pi} \exp \left[-\delta_{QD} \left\{ \left(P - \frac{1}{\delta_{CC}} X \right)^2 + X^2 \right\} \right] \quad ; \quad 0 \leq W \leq \frac{\delta_{QD}}{\pi} \quad (15)$$

where δ_{QD} is referred to as the *degree of quantum decoherence* and δ_{CC} is referred to as the *degree of classical correlations*. The Wigner function is therefore fully characterized by these two dimensionless parameters that capture distinct properties of the quantum state, as outlined below [62]:

- **Degree of Quantum Decoherence** δ_{QD} : This measure coincides with the purity of the reduced density matrix ρ_2 given in (6):

$$\delta_{QD} \equiv \frac{\alpha}{2\gamma} = \text{Tr } \rho_2^2 = \sqrt{\frac{4K_+K_-}{(K_+ + K_-)^2 + (L_+ - L_-)^2}} \quad (16)$$

Consequently, $\delta_{QD} \in [0, 1]$. The upper extreme is saturated by the pure states, for which $\delta_{QD} = 1$. On the other hand, when the effects of an external environment are significant, the state may undergo decoherence, i.e., the non-diagonal entries drop to zero and the reduced density matrix resembles a classical statistical ensemble. This case corresponds to the limit $\delta_{QD} \rightarrow 0$.

- **Degree of Classical Correlations** δ_{CC} : This measure is associated with the sharp-

ness of squeezing of the Wigner function:

$$\begin{aligned}
\delta_{CC} &\equiv \left| \frac{2\alpha\gamma}{\beta} \right| = \frac{\sqrt{K_+K_-[(K_+ + K_-)^2 + (L_+ - L_-)^2]}}{K_+L_- + K_-L_+} \\
&= \frac{2K_+K_-}{K_+L_- + K_-L_+} \sqrt{\frac{[(K_+ + K_-)^2 + (L_+ - L_-)^2]}{4K_+K_-}} \\
&= \frac{1}{\delta_{QD}} \left(\frac{2K_+K_-}{K_+L_- + K_-L_+} \right)
\end{aligned} \tag{17}$$

For the CHO, δ_{CC} is also directly related to the classicality parameter (\mathcal{C}) proposed in [57]. Therein, \mathcal{C} was introduced as a more intuitive measure for quantifying classicality, viz., in terms of the width of the Wigner function around the classical phase-space trajectory. Hence,

$$\mathcal{C} \equiv \frac{\langle xp \rangle_W}{\sqrt{\langle p^2 \rangle_W \langle x^2 \rangle_W}} = \frac{1}{\sqrt{1 + \delta_{CC}^2}} \tag{18}$$

It follows that the classicality parameter $\mathcal{C} \in [0, 1]$ (or $\delta_{CC} \in [0, \infty)$). The lower bound corresponds to the “quantum” limit ($\delta_{CC} \rightarrow \infty$) wherein the Wigner function becomes separable in position and momentum. This follows from the uncertainty principle wherein fixing the value of x can amplify the error in p and vice versa, resulting in probability distributions along x and p that are uncorrelated. On the other hand, the upper bound corresponds to the classical limit ($\delta_{CC} \rightarrow 0$) wherein the Wigner function is no longer separable in x and p , and its peak coincides with well-defined classical phase-space trajectories.

As we remarked earlier, there is a convenient geometrical picture that captures the manner in which the above parameters fully characterize a Gaussian state. To visualize this, consider a particular ‘slice’ of the Wigner function that corresponds to an ellipse in the phase space, referred to as a Wigner ellipse, described below in terms of rotated co-ordinates \tilde{X} and \tilde{P} :

$$\begin{aligned}
\frac{\tilde{X}^2}{a^2} + \frac{\tilde{P}^2}{b^2} &= \frac{1}{\delta_{QD}} \log \frac{\delta_{QD}}{\pi W} \quad ; \quad \begin{bmatrix} \tilde{X} \\ \tilde{P} \end{bmatrix} = \begin{bmatrix} \cos \theta & \sin \theta \\ -\sin \theta & \cos \theta \end{bmatrix} \begin{bmatrix} X \\ P \end{bmatrix} \\
a^2 &= 1 + \frac{1}{2\delta_{CC}^2} \left\{ 1 + \sqrt{1 + 4\delta_{CC}^2} \right\} \\
b^2 &= 1 + \frac{1}{2\delta_{CC}^2} \left\{ 1 - \sqrt{1 + 4\delta_{CC}^2} \right\} \\
\theta &= \sin^{-1} \left[\sqrt{\frac{1}{2} \left\{ 1 + \frac{1}{1 + 4\delta_{CC}^2} \right\}} \right]
\end{aligned} \tag{19}$$

where a and b are the length of semi-major/minor axes of the rotated ellipse and θ is the squeezing angle. A useful such slice of the Wigner function to look at is at the half of its peak, wherein the corresponding ellipse serves as a 2D-generalization of the FWHM (Full-width at Half-maxima) for Gaussian/normal distributions. The equation for the corresponding Wigner ellipse would then take the form:

$$\frac{\tilde{X}^2}{a^2} + \frac{\tilde{P}^2}{b^2} = \frac{\log 2}{\delta_{QD}} \quad (20)$$

When $\delta_{CC} \rightarrow \infty$ (or $\mathcal{C} \rightarrow 0$), we see that the Wigner ellipse reduces to a circle ($a = b = 1$, $\theta = \pi/4$) corresponding to a state that is time-independent or at the beginning of its evolution $t = t_0$.

The phase-space picture of the quantum state can therefore be outlined as follows: (i) Wigner function for the Gaussian state is fully characterized by dimensionless parameters δ_{QD} and δ_{CC} (or \mathcal{C}); (ii) State purity δ_{QD} determines the amplitude features of the Wigner function. For instance, its peak (maxima) and spread (area of the Wigner ellipse at half-maxima) are given by δ_{QD}/π and $\pi \log 2/\delta_{QD}$ respectively; (iii) Classicality parameter \mathcal{C} determines the extent of squeezing (the ratio of semi-major/semi-minor axes a and b) and squeezing angle (θ) of the distribution. From here onwards, we stick to classicality parameter \mathcal{C} as the characteristic measure for squeezing, since it is a fundamental feature of the covariance matrix as we will see in the next subsection, and has a natural extension for large subsystem sizes.

Using this phase-space picture, we may now analyze the conditions required for classicality to emerge in a Gaussian state [15, 62]:

- $\mathcal{C} \rightarrow 1$: In this limit, the Wigner function undergoes a runaway squeezing about the classical phase-space trajectory ($p = \beta x$) of the system.
- $\delta_{QD} \rightarrow 0$: In this limit, the subsystem experiences a runaway decoherence due to its interaction with the environment (here, the other oscillator), causing the amplitude of the Wigner function to fall and spread out over the entire phase space.

It is to be noted that this notion of “classicality” fundamentally differs from taking the formal limit $\hbar \rightarrow 0$ [32]. To illustrate this, let us briefly put back in the Planck’s constant which was set to $\hbar = 1$ and consider the Wigner function as well as the marginal probability

distributions along X and P coordinates separately:

$$\begin{aligned}
W(X, P) &= \frac{\delta_{QD}}{\pi\hbar} \exp \left[-\frac{\delta_{QD}}{\hbar} \left\{ \frac{\tilde{X}^2}{a^2} + \frac{\tilde{P}^2}{b^2} \right\} \right] \quad ; \quad \begin{bmatrix} \tilde{X} \\ \tilde{P} \end{bmatrix} = \begin{bmatrix} \cos \theta & \sin \theta \\ -\sin \theta & \cos \theta \end{bmatrix} \begin{bmatrix} X \\ P \end{bmatrix} \\
f(X) &= \int dP W(X, P) = \frac{1}{\sqrt{2\pi}\sigma_X} \exp \left\{ -\frac{X^2}{2\sigma_X^2} \right\} \quad ; \quad \sigma_X = \sqrt{\frac{\hbar}{2\delta_{QD}}} \\
g(P) &= \int dX W(X, P) = \frac{1}{\sqrt{2\pi}\sigma_P} \exp \left\{ -\frac{P^2}{2\sigma_P^2} \right\} \quad ; \quad \sigma_P = \sqrt{\frac{\hbar}{2\delta_{QD}(1-\mathcal{C}^2)}} \quad (21)
\end{aligned}$$

It is interesting to note here that while purity δ_{QD} affects the variance for distributions in both X and P , classicality parameter \mathcal{C} only affects the variance in P . The measurement error in the (x, p) -coordinates is therefore:

$$\sigma_x \sigma_p = \sigma_X \sigma_P = \frac{\hbar}{2\delta_{QD}\sqrt{1-\mathcal{C}^2}} \geq \frac{\hbar}{2} \quad (22)$$

We see that the uncertainty principle is saturated when $\delta_{QD} = 1$ and $\mathcal{C} = 0$, corresponding to a pure-state at $t = t_0$. The classical limit $\hbar \rightarrow 0$, as seen from above, corresponds to the case where the uncertainty (as well as the commutator of conjugate variables) vanishes, and the phase-space distributions are highly localized (δ -functions) [15, 63]:

$$W \rightarrow \delta \left(\frac{\tilde{X}}{a} \right) \delta \left(\frac{\tilde{P}}{b} \right) \quad ; \quad f \rightarrow \delta(X) \quad ; \quad g \rightarrow \delta(P) \quad (23)$$

Morikawa's classicality criteria on the other hand points to a divergent uncertainty in both x and p measurements, wherein the phase-space distributions are less and less localized (Fig. 1). Despite this contrast, Morikawa's criteria leads to a notion of "quasi-classicality" [15] *within* the framework of quantum mechanics in the following sense — i) decoherence essentially leads to a (reduced) density matrix that resembles a classical statistical ensemble, and ii) squeezing further aligns the peaks of (reduced) Wigner function along classical phase-space trajectories. The overall implication is that the features that make a state *distinctly* quantum are greatly suppressed. For instance, let us look at the Wigner-Weyl transform of the following observables whose expectation values are to be calculated via (13):

$$\begin{aligned}
\mathcal{W} [\hat{x}\hat{p} + \hat{p}\hat{x}] &= \mathcal{W} [2\mathcal{S}(\hat{x}\hat{p})] = 2xp \\
\mathcal{W} [\hat{x}^2\hat{p}^2 + \hat{p}^2\hat{x}^2] &= \mathcal{W} [2\mathcal{S}(\hat{x}^2\hat{p}^2) + [\hat{x}, \hat{p}]^2] = 2x^2p^2 - \hbar^2 \\
\mathcal{W} [f(\hat{x}, \hat{p})] &= \mathcal{W} [\mathcal{S}(f(\hat{x}, \hat{p})) + g([\hat{x}, \hat{p}])] = f(x, p) + \tilde{g}(\hbar), \quad (24)
\end{aligned}$$

where \mathcal{S} is a symmetrizer for combinations of \hat{x} and \hat{p} operators, and satisfies $\mathcal{W}[\mathcal{S}(\hat{x}^n \hat{p}^m)] = x^n p^m$ [64, 65]. The Weyl-transform of a Hermitian, polynomial combination $f(\hat{x}, \hat{p})$ of conjugate variables is therefore real-valued phase-space functions that can be split into a “classical” contribution (from the symmetrizer) and a “quantum” contribution (from the commutator) [61]. Since all higher-order correlators are polynomial functions of two-point correlators for a Gaussian state, it is sufficient to perform a comparison using expectation values of the commutator and the anti-commutator (i.e., symmetrizer at second order):

$$R_{(x,p)} \equiv \left| \frac{\langle [\hat{x}, \hat{p}] \rangle}{\langle \{\hat{x}, \hat{p}\} \rangle} \right| = \delta_{QD} \delta_{CC} = \frac{\delta_{QD}}{\mathcal{C}} \sqrt{1 - \mathcal{C}^2}, \quad (25)$$

The above ratio compares the strength of quantum and classical contributions over the course of state evolution [22]. We see that Morikawa’s classicality criteria ($\delta_{QD} \rightarrow 0$ and $\mathcal{C} \rightarrow 1$) leads to an *extremely rapid* suppression of non-commutativity, in favour of the aforementioned notion of quasi-classicality. This further implies that even if we are able to somehow measure observables that directly capture quantum signatures as in (24), these signatures will be tremendously suppressed by squeezing and/or decoherence, leaving little room to distinguish between a quantum and classical origin for observations. It is also to be noted that the classicality criteria places *stronger* conditions than $R_{(x,p)} \rightarrow 0$, requiring simultaneous decoherence ($\delta_{QD} \rightarrow 0$) *and* squeezing ($\mathcal{C} \rightarrow 1$). We again set $\hbar = 1$ for the rest of the paper, and in the next subsection we will see how the classicality criteria can be reconciled with a stability analysis of the quantum state in the phase-space.

B. Phase space stability analysis

The vacuum states are typically well-defined when the Hamiltonian becomes time-independent. Hence in the case of CHO we consider an evolution in $\omega(t)$ and $\chi(t)$ that are asymptotically constant. In Ref. [45], the authors showed that the asymptotic values of the normal modes decided the late-time stability of the system, the signatures of which were obtained from various correlation measures. Similarly, we may consider the stability analysis of the quantum state in the phase-space via the Wigner function. Let us set the values of the two normal modes — $\omega_+^2(t) = \omega^2(t)$ and $\omega_-^2(t) = \omega^2(t) + 2\chi^2(t)$ — to constant values u_+^2 and u_-^2 ($u_+^2 \leq u_-^2$), respectively at late-times. In the asymptotic future ($t \rightarrow \infty$),

the Ermakov equation, therefore, takes the following form:

$$\ddot{b}_j(t) + u_j^2 b_j(t) \sim \frac{\omega_j^2(t_0)}{b_j^3(t)} \quad ; \quad j = +, - \quad (26)$$

Since the co-efficient in the second term of the above equation is time-independent, we can obtain the following solutions [66]:

$$b_j(t) \sim \sqrt{1 + \left(\frac{\omega_j^2(t_0)}{u_j^2} - 1 \right) \sin^2 u_j t} \quad ; \quad \dot{b}_j(t) \sim (\omega_j^2(t_0) - u_j^2) \frac{\sin 2u_j t}{2u_j b_j(t)}. \quad (27)$$

We now look at various stability regimes of these solutions below and track its features in the phase-space picture (see Fig. 1) :

- Stable Modes $u_j^2 > 0$: Scaling parameters $\{b_j\}$ are oscillatory and bounded.
- Zero Modes $u_j^2 = 0$:

$$b_j(t) \sim \omega_j(t_0)t \quad ; \quad \dot{b}_j(t) \sim \omega_j(t_0) \quad (28)$$

Suppose ω_+ is a zero mode and ω_- is a stable mode. At late-times, we have:

$$\delta_{QD} \sim \frac{2}{t} \sqrt{\frac{K_-}{(K_-^2 + L_-^2)\omega_+(t_0)}} \quad ; \quad \mathcal{C} \sim \frac{1}{\sqrt{1 + \frac{K_-^2 + L_-^2}{K_- \omega_+(t_0)}}} \quad (29)$$

We see that the purity falls to zero as $t \rightarrow \infty$, whereas classicality parameter retains its oscillatory behaviour about a value between 0 and 1, i.e., there is no runaway squeezing.

- Inverted Modes $u_j^2 < 0$: At late times, the solutions (27) further reduce to :

$$b_j(t) \sim c_j e^{v_j t} \quad ; \quad \dot{b}_j(t) \sim c_j v_j e^{v_j t} \quad ; \quad c_j = \frac{1}{2} \sqrt{1 + \frac{\omega_j^2(t_0)}{v_j^2}} \quad (30)$$

where we have defined $u_j = iv_j$. When both modes are inverted, we see that $v_+ \geq v_-$ in general, and as a result:

$$\lim_{t \rightarrow \infty} \delta_{QD} \sim \begin{cases} \frac{2\sqrt{\omega_+(t_0)\omega_-(t_0)}}{c_+ c_- (v_+ - v_-)} e^{-(v_+ + v_-)t} & v_+ > v_- \\ \frac{2c_+ c_- \sqrt{\omega_+(t_0)\omega_-(t_0)}}{c_+^2 \omega_-(t_0) + c_-^2 \omega_+(t_0)} & v_+ \rightarrow v_- \end{cases} \quad (31)$$

The result gives us two distinct cases — if $v_+ > v_-$ (gapped), the long-time limit will always result in a purity that exponentially decays to zero, thereby exhibiting rapid

decoherence. On the other hand, if the inverted modes converge asymptotically (i.e., ungapped), the subsystem is protected from further decoherence (this conditions for purity saturation is much more general, as worked out in Appendix A). The degree of classical correlation δ_{CC} , on the other hand, has the following late-time behaviour:

$$\lim_{t \rightarrow \infty} \mathcal{C}^2 \sim \begin{cases} 1 - \frac{\omega_+(t_0)c_-^2}{\omega_-(t_0)c_+^2} \left(1 - \frac{v_-}{v_+}\right)^2 e^{-2(v_+ - v_-)t} & v_+ > v_- \\ 1 - \frac{\omega_+(t_0)\omega_-(t_0)}{c_+^2 c_-^2 v^2} e^{-4vt} & v_+ \rightarrow v_- \sim v \end{cases} \quad (32)$$

We see that at late times $\mathcal{C} \rightarrow 1$, with the squeezing being much faster in the ungapped case than in the gapped case. Therefore, we see that the only case that simultaneously results in both rapid decoherence and runaway squeezing, thereby satisfying the classicality criteria, is when the system develops gapped inverted modes.

From Fig. 1 and Table I, we see that for the CHO the only case that asymptotically satisfies the classicality criteria is when the modes are inverted and gapped. Here, the inverted modes cause an exponentially fast suppression of non-commutativity as per (25). Interestingly, we see that this is also the only regime where entanglement entropy ($S = -\text{Tr } \rho_{red} \log \rho_{red}$) mimics its classical counterpart, the Kolmogorov-Sinai entropy [45, 67]:

$$S(t) \sim h_{KS} t \quad ; \quad h_{KS} = \sum_i \lambda_i, \quad (33)$$

where growth rate h_{KS} is the sum of all positive Lyapunov exponents. Therefore, we may argue that this is indeed the regime where an asymptotic quantum-classical transition occurs in the case of a CHO. While Morikawa's criteria in CHO has been explored to varying extents in previous works [15, 68, 69], our approach reconciles it with a stability analysis of the quantum state in its phase-space representation, in a way that is also scale-able to larger subsystem sizes. To the best of our knowledge, this criterion has not been extended in this way, and we will describe how to calculate it in next subsection.

C. Classicality criteria for N oscillators

For a system of N oscillators, the reduced density matrix after integrating out m oscillators will have the following form as derived in Appendix C:

$$\rho_{out} = \sqrt{\frac{\det\{1 - \Gamma_D\}}{\pi^{N-m}}} \exp \left\{ -Y^T \left(\frac{1 - i\tilde{\Gamma}_3}{2} \right) Y - Y'^T \left(\frac{1 + i\tilde{\Gamma}_3}{2} \right) Y' + Y'^T \Gamma_D Y \right\}, \quad (34)$$

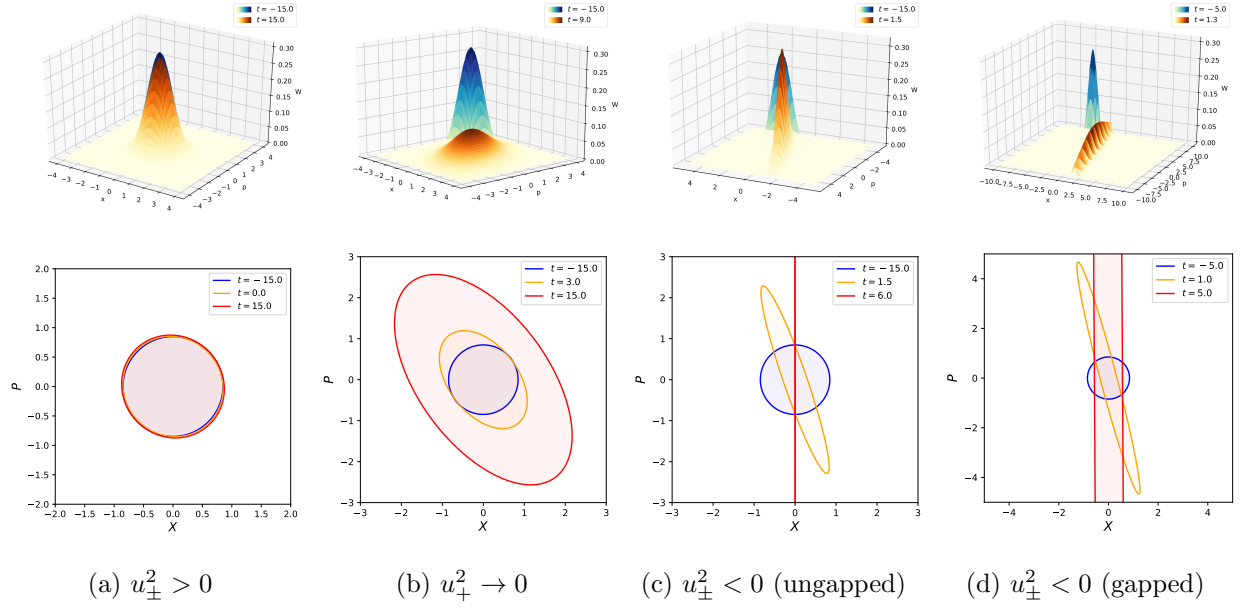


FIG. 1: Evolution of Wigner function (Row 1) and Wigner ellipse at half-maximum (Row 2) for the CHO when $\omega^2(t)$ evolves as (90) with $Q = 1$ and $a_0 = 1$ with constant coupling $\chi(t) = 1$ (except for (c)) — (a) $a_1 = 0.5$ results in stable modes showing little deviation from the initial “highly quantum” vacuum state, (b) $a_1 = 0$ results in a zero mode that decoheres the subsystem but limits the squeezing, (c) $a_1 = -0.5$ with $\chi^2(t) = e^{-(t-ti)}$ results in ungapped inverted modes that squeeze the state but limit the decoherence, and (d) $a_1 = -2.5$ results in gapped inverted modes that both squeeze and decohere the state, signifying a quantum-classical transition.

Asymptotics	$\delta_{QD} \not\rightarrow 0$	$\delta_{QD} \rightarrow 0$
$\mathcal{C} \not\rightarrow 1$	Stable modes ($u_{\pm}^2 > 0$) $[R_{(x,p)} \not\rightarrow 0]$	Zero mode ($u_{\pm}^2 \rightarrow 0$) $[R_{(x,p)} \rightarrow 0]$
$\mathcal{C} \rightarrow 1$	Inverted modes ($u_{\pm}^2 < 0$) Case 1 : $v_+ \rightarrow v_-$ $[R_{(x,p)} \rightarrow 0]$	Inverted modes ($u_{\pm}^2 < 0$) Case 2 : $v_+ \neq v_-$ $[R_{(x,p)} \rightarrow 0]$

TABLE I: Testing classicality criteria for various stability regimes in CHO.

where,

$$\Gamma = W^T \Gamma_D W \quad \tilde{\Gamma}_3 = W \gamma_D^{-1/2} V \Gamma_3 V^T \gamma_D^{-1/2} W^T. \quad (35)$$

and

$$\begin{aligned} \Gamma_1 &= C - \frac{1}{2} B^T A^{-1} B + \frac{1}{2} Z_B^T A^{-1} Z_B \\ \Gamma_2 &= \frac{1}{2} B^T A^{-1} B + \frac{1}{2} Z_B^T A^{-1} Z_B \\ \Gamma_3 &= Z_C - Z_B^T A^{-1} B \end{aligned} \quad (36)$$

The Wigner function for the $N - m$ reduced oscillator system is given by:

$$\begin{aligned} W(X, P) &= \frac{1}{(2\pi)^{N-m}} \int_{-\infty}^{\infty} dx_{\Delta} \rho \left(X - \frac{x_{\Delta}}{2}, X + \frac{x_{\Delta}}{2} \right) e^{-iP^T x_{\Delta}} \\ &= \frac{\Delta_{QD}^{1/2}}{\pi^{N-m}} \exp \left[-X^T (1 - \Gamma_D) X - \left\{ P^T - X^T \tilde{\Gamma}_3 \right\} \frac{1}{1 + \Gamma_D} \left\{ P - \tilde{\Gamma}_3 X \right\} \right], \end{aligned} \quad (37)$$

where we obtain the purity spectrum $\delta_{QD}^{(j)}$ of the reduced state in the basis that diagonalizes the Γ matrix, along with the overall purity Δ_{QD} :

$$\delta_{QD}^{(j)} = \sqrt{\frac{1 - (\Gamma_D)_{jj}}{1 + (\Gamma_D)_{jj}}} \quad ; \quad \Delta_{QD} = \prod_j \delta_{QD}^{(j)} \quad (38)$$

While the overall purity Δ_{QD} of the reduced state appears to be a natural extension of the measure δ_{QD} in CHO, the *entanglement entropy* of the subsystem is a richer measure of decoherence for larger subsystem sizes [70]. The entanglement entropy for the subsystem is obtained as follows [35, 45]:

$$S = \sum_{j=m+1}^N S_j \quad ; \quad S_j = -\log[1 - \xi_j] - \frac{\xi_j}{1 - \xi_j} \log \xi_j \quad ; \quad \xi_j = \frac{1 - \delta_{QD}^{(j)}}{1 + \delta_{QD}^{(j)}} \quad (39)$$

The key to reformulating the classicality criteria for large subsystem sizes lies in the *covariance matrix* of the reduced system. This is because for Gaussian states, all information about correlations are captured in the covariance matrix, which can be effectively used to measure both decoherence as well as squeezing even for large system sizes. In order to see this, let us first write down the covariance matrix corresponding to the reduced Wigner function as follows [4]:

$$\Sigma = \begin{bmatrix} \sigma_{XX} & \sigma_{XP} \\ \sigma_{XP}^T & \sigma_{PP} \end{bmatrix} ; (\sigma_{XX})_{ij} = \langle \{x_i, x_j\} \rangle ; (\sigma_{XP})_{ij} = \langle \{x_i, p_j\} \rangle ; (\sigma_{PP})_{ij} = \langle \{p_i, p_j\} \rangle \quad (40)$$

Upon evaluating the correlators, we obtain the following matrix elements:

$$(\sigma_{XX})_{ij} = \frac{\delta_{ij}}{1 - \Gamma_j} \quad ; \quad (\sigma_{XP})_{ij} = \frac{(\tilde{\Gamma}_3)_{ij}}{1 - \Gamma_i} \quad ; \quad (\sigma_{PP})_{ij} = (1 + \Gamma_j)\delta_{ij} + \sum_k \frac{(\tilde{\Gamma}_3)_{ik}(\tilde{\Gamma}_3)_{jk}}{1 - \Gamma_k} \quad (41)$$

Writing down the conditional covariance matrix [71] for the reduced system is a useful step towards identifying decoherence from the covariance matrix:

$$\Sigma_{P|X} = \sigma_{PP} - \sigma_{XP}^T \sigma_{XX}^{-1} \sigma_{XP} \quad ; \quad (\Sigma_{P|X})_{ij} = (1 + \Gamma_j)\delta_{ij} \quad (42)$$

It is now easy to see that the $N \times N$ block determinant matrix $(\det \Sigma)$ for the $2N \times 2N$ covariance matrix gives the purity spectrum:

$$[\det \Sigma]_{ij} = \left[\sigma_{XX}^{1/2} \Sigma_{P|X} \sigma_{XX}^{1/2} \right]_{ij} = \frac{\delta_{ij}}{[\delta_{QD}^{(j)}]^2} = \lambda_j \delta_{ij} \quad (43)$$

The entanglement entropy is therefore related to the eigenvalues $\{\lambda_j\}$ of the block determinant $(\det \Sigma)$ as follows, consistent with the expression in (39):

$$S = \sum_{j=1}^{N-m} S_j \quad ; \quad S_j = \left(\frac{\sqrt{\lambda_j} + 1}{2} \right) \log \left(\frac{\sqrt{\lambda_j} + 1}{2} \right) - \left(\frac{\sqrt{\lambda_j} - 1}{2} \right) \log \left(\frac{\sqrt{\lambda_j} - 1}{2} \right) \quad (44)$$

On the other hand, in order to generalize the classicality parameter (that measures squeezing of the Wigner function) for large subsystem sizes, let us first look at the determinant of the reduced covariance matrix for the CHO using (14):

$$\frac{1}{4} (\det \Sigma)_{red} = \langle x^2 \rangle \langle p^2 \rangle - \langle xp \rangle^2 = \frac{1}{4\delta_{QD}^2} \quad (45)$$

Upon rescaling this by $\langle x^2 \rangle \langle p^2 \rangle$ and rearranging using (18), we get:

$$\mathcal{C} = \sqrt{1 - \frac{1}{4\langle x^2 \rangle \langle p^2 \rangle \delta_{QD}^2}} = \sqrt{1 - \frac{\det \Sigma_{red}}{\sigma_{XX} \sigma_{PP}}} \quad (46)$$

We now generalize this measure in terms of *classicality matrix* C defined as follows, and propose it as a powerful tool towards quantifying the extent of squeezing in a multi-mode covariance matrix:

$$\begin{aligned} C &= \sqrt{1 - [\sigma_{XX}^{1/2} \sigma_{PP} \sigma_{XX}^{1/2}]^{-1/2} (\det \Sigma) [\sigma_{XX}^{1/2} \sigma_{PP} \sigma_{XX}^{1/2}]^{-1/2}} \\ &= \sqrt{[\sigma_{XX}^{1/2} \sigma_{PP} \sigma_{XX}^{1/2}]^{-1/2} \sigma_{XX}^{1/2} \sigma_{XP}^T \sigma_{XX}^{-1} \sigma_{XP} \sigma_{XX}^{1/2} [\sigma_{XX}^{1/2} \sigma_{PP} \sigma_{XX}^{1/2}]^{-1/2}} \end{aligned} \quad (47)$$

The above matrix captures the relative contribution of the off-diagonal blocks σ_{XP} and σ_{PX} with respect to the diagonal blocks σ_{XX} and σ_{PP} in the covariance matrix, i.e., it measures how sharply the multi-variate reduced Wigner function squeezes. For the case of CHO, the above result reduces to (18). However, for a larger subsystem size, we construct its determinant (a matrix invariant) using the eigenvalues $\{C_j\}$. In order to have a better comparison with entanglement entropy of the same subsystem, we further rewrite the determinant in terms of what we refer from here on out as “log classicality” $LC(t)$:

$$\mathcal{C} = \prod_j C_j \quad ; \quad LC = -\log \sqrt{1 - \mathcal{C}^2}, \quad (48)$$

The above measure is well-behaved, and is a characteristic feature of a multi-mode covariance matrix. Entanglement entropy and log classicality are therefore insightful single-valued measures that extract the extent of decoherence and squeezing directly from the covariance matrix associated with a given (multi-mode) quantum state. The criteria for asymptotic quantum-classical transition can hence be reformulated for large subsystem sizes as follows:

$$\lim_{t \rightarrow \infty} S \rightarrow \infty \quad ; \quad \lim_{t \rightarrow \infty} LC \rightarrow \infty \quad (49)$$

In the above limit, a multi-mode generalization for the ratio defined in (25) is also expected to vanish. However, since it is a weaker requirement for classicality than (49), we do not address such a generalization in this work.

For CHO, we see that the inverted modes lead to the following leading order behaviour at late-times, with only the gapped ($v_+ > v_-$) case satisfying the classicality criteria:

$$\lim_{t \rightarrow \infty} S \sim \begin{cases} (v_+ + v_-)t & v_+ > v_- \\ const. & v_+ \rightarrow v_- \end{cases} \quad ; \quad \lim_{t \rightarrow \infty} LC \sim \begin{cases} (v_+ - v_-)t & v_+ > v_- \\ 2v_{\pm}t & v_+ \rightarrow v_- \end{cases} \quad (50)$$

Having successfully generalized the classicality criteria for multi-mode Gaussian states, we may now utilize this to identify quantum-classical transition in physical scenarios modeled by dynamically evolving harmonic lattices. The criteria, however, may have a possible caveat — even for a fixed bipartition, it depends on the choice of conjugate variables and is subject to change under canonical transformations. We will address this in much detail in the next section before proceeding to early-Universe fluctuations.

III. CLASSICALITY CRITERIA AND CANONICAL TRANSFORMATIONS

In general, a scalar field propagating in a background space-time may be quantized in different co-ordinate settings. The respective conjugate variables are related via canonical transformations, and ideally we require a classicality criteria that is independent of the choice of these variables. While a lot of progress has been made in identifying quantum-classical transition particularly in the two-mode squeezed-state representation in the momentum space [15, 27, 28], the choice of conjugate variables is found to play a crucial role, i.e., a system identified as “classical” can be made “quantum” with a simple canonical transformation [72]. Similarly, while in Section II we were able to successfully extend Morikawa’s classicality criteria to multi-mode Gaussian states, we see in this section that it is not completely independent of the choice of conjugate variables either.

A. Time-dependent Harmonic Oscillator

To investigate the effects of canonical transformations, let us consider the Hamiltonian of a time-dependent oscillator as follows:

$$\mathcal{H}^{(I)}(\eta) = \frac{P^2}{2} + \frac{\omega_I^2(\eta)X^2}{2} = \frac{P^2}{2} + \frac{a^2(\eta)\Omega^2(\eta)X^2}{2}, \quad (51)$$

where we now use η as the time coordinate for comparison. The wave-function that describes the system is a solution to the time-dependent Schrödinger equation, and unitarily evolves from an initial state defined at $\eta = \eta_0$ as follows [55, 73]:

$$\Psi(\eta) = \exp\left\{-i \int_{\eta_0}^{\eta} \mathcal{H}^{(I)}(\eta') d\eta'\right\} \Psi(\eta_0) \quad (52)$$

Let us now transform the Hamiltonian $\mathcal{H}^{(I)}(\eta) \rightarrow \mathcal{H}^{(II)}(\eta)$ as follows:

$$\mathcal{H}^{(II)}(t) = \frac{\mathcal{H}^{(I)}(\eta(t))}{a(\eta(t))} = \frac{P^2}{2a(\eta(t))} + \frac{a(\eta(t))\Omega^2(\eta(t))X^2}{2} \quad (53)$$

With the above rescaling, the time-evolution of a particular state can be preserved by also rescaling the time-coordinate appropriately:

$$\int_{\eta_0}^{\eta} \mathcal{H}^{(I)}(\eta) d\eta = \int_{t_0}^t \mathcal{H}^{(II)}(t) dt \quad ; \quad t = \int a(\eta) d\eta \quad (54)$$

Now, we employ the following canonical transformations with respect to $\mathcal{H}^{(II)}$ [74]:

$$X = \frac{x}{\sqrt{a(t)}} \quad ; \quad P = \sqrt{a(t)}p - \frac{\dot{a}(t)}{2\sqrt{a(t)}}x \quad (55)$$

The resultant Hamiltonian is:

$$\mathcal{H}^{(II)}(t) = \frac{p^2}{2} + \frac{\omega_{II}^2(t)x^2}{2} \quad ; \quad \omega_{II}^2(t) = \frac{\omega_I^2(\eta(t))}{a^2(t)} + \frac{1}{4} \left(\frac{\dot{a}(t)}{a(t)} \right)^2 - \frac{\ddot{a}(t)}{2a(t)} \quad (56)$$

We now look at how the scaling parameters corresponding to $\mathcal{H}^{(I)}$ and $\mathcal{H}^{(II)}$, namely $B(\eta)$ and $b(t)$ are related. For this, we look at the non-linear Ermakov equation:

$$B''(\eta) + \omega_I^2(\eta)B(\eta) = \frac{\omega_I^2(\eta_0)}{B^3(\eta)} \quad (57)$$

To arrive at a solution for the Ermakov equation, we first consider solutions to the classical time-dependent oscillator:

$$Y''(\eta) + \omega_I^2(\eta)Y(\eta) = 0 \quad (58)$$

From a set of independent solutions $Y_1(\eta)$ and $Y_2(\eta)$ of the above equation, the scaling parameter $B(\eta)$ can be obtained as follows:

$$B^2(\eta) = \frac{1}{W_Y^2} \left[\{Y_1(\eta)Y_2'(\eta_0) - Y_1'(\eta_0)Y_2(\eta)\}^2 + \omega_I^2(\eta_0) \{Y_1(\eta)Y_2(\eta_0) - Y_2(\eta)Y_1(\eta_0)\}^2 \right], \quad (59)$$

where W_Y is the Wronskian for solutions $Y_1(\eta)$ and $Y_2(\eta)$, which is here time-independent. The above solution automatically satisfies the initial conditions $B(\eta_0) = 1$ and $B'(\eta_0) = 0$ *regardless* of the initial conditions chosen for Y_1 and Y_2 .

Similarly, for Hamiltonian $\mathcal{H}^{(II)}$, we write down the classical equation of motion and Ermakov equations respectively as follows:

$$\ddot{y}(t) + \omega_{II}^2(t)y(t) = 0 \quad ; \quad \ddot{b}(t) + \omega_{II}^2(t)b(t) = \frac{\omega_{II}^2(t_0)}{b^3(t)} \quad (60)$$

Suppose the independent solutions are $y_1(t)$ and $y_2(t)$, the scaling parameter $b(t)$ are obtained as follows:

$$b^2(t) = \frac{1}{W_y^2} \left[\{y_1(t)\dot{y}_2(t_0) - \dot{y}_1(t_0)y_2(t)\}^2 + \omega_{II}^2(t_0) \{y_1(t)y_2(t_0) - y_2(t)y_1(t_0)\}^2 \right], \quad (61)$$

where W_y is the Wronskian for solutions $y_1(t)$ and $y_2(t)$. The above solution automatically satisfies the initial conditions $b(t_0) = 1$ and $\dot{b}(t_0) = 0$. Using the equation connecting frequencies $\omega_I^2(t)$ and $\omega_{II}^2(\eta)$ in (56), we obtain the following relations connecting $y(t)$ and $Y(\eta)$:

$$y(t) = \sqrt{a(t)}Y(\eta(t)) \quad ; \quad \dot{y}(t) = \frac{1}{\sqrt{a(t)}} \left(Y'(\eta(t)) + \frac{\dot{a}(t)}{2}Y(\eta(t)) \right); \quad W_y = W_Y \quad (62)$$

Substituting this back into the solution $b(t)$, we obtain the following relation:

$$b^2(t) = \frac{a(t)}{a(t_0)} B^2(\eta) + \frac{a(t)a(t_0)}{2W_Y^2} \left\{ \frac{\dot{a}^2(t_0)}{a^2(t_0)} - \frac{\ddot{a}(t_0)}{a(t_0)} \right\} [Y_1(\eta)Y_2(\eta_0) - Y_1(\eta_0)Y_2(\eta)]^2 \\ + \frac{a(t)\dot{a}(t_0)}{W_Y^2 a(t_0)} [Y_1(\eta)Y_2'(\eta_0) - Y_1'(\eta_0)Y_2(\eta)] [Y_1(\eta)Y_2(\eta_0) - Y_1(\eta_0)Y_2(\eta)] \quad (63)$$

The above expression relates the time-evolution from the respective vacuum states corresponding to $\mathcal{H}^{(I)}$ and $\mathcal{H}^{(II)}$. Alternatively, one may be interested in studying the evolution of, say, the η -vacuum in the t representation (see, for instance, [58]). This leads to a simplified relation between the corresponding scaling parameters. To see this, notice that the wave functions, in the two different representations, of a given state of the system are related via:

$$\Psi_{II}(x, t) = \frac{1}{a^{1/4}(t)} \Psi_I[X(x), \eta(t)] \exp \left\{ i \frac{\dot{a}(t)}{4a(t)} x^2 \right\} \quad (64)$$

For the special case of a Gaussian state, the above relation translates to the following relation between the corresponding scaling parameters:

$$\frac{\omega_{II}(t_0)}{b^2(t)} = \frac{\omega_I(\eta_0)}{a(t)B^2(\eta)} \quad ; \quad \frac{\dot{b}(t)}{b(t)} = \frac{1}{a(t)} \left[\frac{B'(\eta(t))}{B(\eta(t))} + \frac{\dot{a}(t)}{2} \right] \quad (65)$$

Consequently, the above relation is also valid if one can further specialize to the vacuum state of one of the representations. The relevance of this relation is that its direct extension to the case of harmonic lattices can be used to study the consequences of canonical transformations. Note that in the limit

$$\dot{a}(t_0) \rightarrow 0 \quad \text{and} \quad \ddot{a}(t_0) \rightarrow 0 \quad (66)$$

we obtain (65) from (63). This limit, therefore, translates to the case when the instantaneous vacua of both representations coincide at $t = t_0$.

B. Time-dependent CHO

In order to observe the effects of canonical transformations on the classicality criteria, we now look at the CHO:

$$\mathcal{H}^{(I)}(\eta) = \frac{P_1^2}{2} + \frac{P_2^2}{2} + \frac{1}{2}\omega_I^2(\eta) (X_1^2 + X_2^2) + \frac{1}{2}\chi_I^2(\eta) (X_1 - X_2)^2 \quad ; \quad \mathcal{H}^{(II)} = \frac{\mathcal{H}^{(I)}[\eta(t)]}{a[\eta(t)]} \quad (67)$$

The canonical transformations in (55) result in the following Hamiltonian:

$$\mathcal{H}^{(II)}(t) = \frac{p_1^2}{2} + \frac{p_2^2}{2} + \frac{1}{2}\omega_{II}^2(t)(x_1^2 + x_2^2) + \frac{1}{2}\chi_{II}^2(t)(x_1^2 - x_2^2) \quad (68)$$

$$\omega_{II}^2(t) = \frac{\omega_I^2[\eta(t)]}{a^2(t)} + \frac{1}{4} \left(\frac{\dot{a}(t)}{a(t)} \right)^2 - \frac{\ddot{a}(t)}{2a(t)} \quad (69)$$

$$\chi_{II}^2(t) = \frac{\chi_I^2[\eta(t)]}{a^2(t)} \quad (70)$$

In terms of K_{\pm} and L_{\pm} defined with respect to Hamiltonians $\mathcal{H}^{(I)}$ and $\mathcal{H}^{(II)}$ as given in (7), we get:

$$K_{\pm}^{(II)}(t) = \frac{K_{\pm}^{(I)}[\eta(t)]}{a(t)} \quad ; \quad L_{\pm}^{(II)}(t) = \frac{1}{a(t)} \left(L_{\pm}^{(I)}[\eta(t)] + \frac{\dot{a}(t)}{2} \right) \quad (71)$$

We now look at how the characteristic parameters of the Wigner function are affected upon going from $\mathcal{H}^{(I)}$ described in terms of time η to $\mathcal{H}^{(II)}$ described in terms of time t :

- Degree of Quantum Decoherence δ_{QD} :

$$\begin{aligned} \delta_{QD}^{(II)}(t) &= \sqrt{\frac{4K_+^{(II)}(t)K_-^{(II)}(t)}{(K_+^{(II)}(t) + K_-^{(II)}(t))^2 + (L_+^{(II)}(t) - L_-^{(II)}(t))^2}} \\ &= \sqrt{\frac{4K_+^{(I)}[\eta(t)]K_-^{(I)}[\eta(t)]}{(K_+^{(I)}[\eta(t)] + K_-^{(I)}[\eta(t)])^2 + (L_+^{(I)}[\eta(t)] - L_-^{(I)}[\eta(t)])^2}} = \delta_{QD}^{(I)}[\eta(t)]. \end{aligned} \quad (72)$$

- Degree of Classical Correlation δ_{CC} :

$$\begin{aligned} \frac{1}{\delta_{CC}^{(II)}(t)} &= \frac{K_+^{(II)}(t)L_-^{(II)}(t) + K_-^{(II)}(t)L_+^{(II)}(t)}{\sqrt{K_+^{(II)}(t)K_-^{(II)}(t) \left[(K_+^{(II)}(t) + K_-^{(II)}(t))^2 + (L_+^{(II)}(t) - L_-^{(II)}(t))^2 \right]}} \\ &= \frac{1}{\delta_{CC}^{(I)}(\eta)} \left[1 + \left(\frac{\dot{a}(t)}{2} \right) \frac{K_+^{(I)}[\eta(t)] + K_-^{(I)}[\eta(t)]}{K_+^{(I)}[\eta(t)]L_-^{(I)}[\eta(t)] + K_-^{(I)}[\eta(t)]L_+^{(I)}[\eta(t)]} \right] \end{aligned} \quad (73)$$

Upon plugging the above expressions into (17) and (39), we see that entanglement entropy (being a symplectic invariant [70]) stays invariant under the canonical transformation in (55), whereas log classicality does not:

$$S^{(II)}(t) = S^{(I)}(\eta(t)) \quad ; \quad LC^{(II)}(t) \neq LC^{(I)}(\eta(t)) \quad ; \quad t = \int a(\eta) d\eta \quad (74)$$

For the special case where $a(t) = a_0$ (constant), however, we see that they are both invariant [45]:

$$S^{(II)}(t) = S^{(I)}(a_0^{-1}t) \quad ; \quad LC^{(II)}(t) = LC^{(I)}(a_0^{-1}t) \quad ; \quad t = a_0\eta \quad (75)$$

The classicality criteria therefore has an ambiguity — the condition on classicality parameter \mathcal{C} is subject to change under a canonical transformation, even for the same time-evolved state, and the same subsystem division. Therefore, in order to manage this ambiguity, we make the second condition stronger by claiming that both representations $\mathcal{H}^{(I)}$ and $\mathcal{H}^{(II)}$ must satisfy the classicality criteria in (49),

$$\lim_{t \rightarrow \infty} S \rightarrow \infty \quad ; \quad \lim_{t \rightarrow \infty} LC \rightarrow \infty,$$

failing which an asymptotic quantum-classical transition may be ruled out. Having amended the classicality criteria this way, we will now proceed to analyze early-Universe fluctuations in the following sections.

IV. EARLY UNIVERSE FLUCTUATIONS IN $(1+1) - D$

In this section, we apply the classicality criteria developed in Sections II and III for fluctuations propagating in an expanding universe in $(1+1)$ -dimensions. Although this does not reflect the physical situation that concerns us, the extensive analytic control we have compared to $(3+1)$ -dimensions can provide us with valuable insight on how an expanding background affects the “quantumness” of such fluctuations. The unperturbed FLRW metric in comoving coordinates clocked by cosmic time (\tilde{t}) and conformal time ($\tilde{\eta}$) are respectively given below:

$$ds^2 = d\tilde{t}^2 - a^2(\tilde{t})d\tilde{x}^2 = a^2(\tilde{\eta}) [d\tilde{\eta}^2 - d\tilde{x}^2] \quad ; \quad d\tilde{t} = a(\tilde{\eta})d\tilde{\eta} \quad (76)$$

The action for a massive test scalar field in an arbitrary space-time background is given below:

$$S = \frac{1}{2} \int d\tilde{x}^\mu \sqrt{-g} \left[g^{\mu\nu} \partial_\mu \tilde{\Phi} \partial_\nu \tilde{\Phi} - \tilde{m}_f^2 \tilde{\Phi}^2 \right] \quad (77)$$

In $(1+1)$ -dimensions, the above action reduces to [75]:

$$S = \int d\tilde{t} L \quad ; \quad L = \frac{1}{2} \int d\tilde{x} \left[\tilde{\Phi}'^2 - (\partial_x \tilde{\Phi})^2 - \tilde{m}_f^2 \tilde{\Phi}^2 \right] \quad (78)$$

Upon defining the canonical momentum as $\tilde{\Pi} = \partial_{\tilde{\Phi}} L$, and discretizing the system as $\tilde{x} = j\tilde{d}$, we get:

$$\mathcal{H}[\tilde{\eta}] = \frac{1}{2\tilde{d}} \sum_j \left[\tilde{\Pi}_j^2 + \left\{ \tilde{\Phi}_j - \tilde{\Phi}_{j+1} \right\}^2 + \tilde{d}^2 \tilde{m}_f^2 a^2(\tilde{\eta}) \tilde{\Phi}_j^2 \right] = \frac{\mathcal{H}^{(I)}}{\tilde{d}} \quad (79)$$

We now absorb the UV cutoff \tilde{d} via appropriate canonical transformations [45]:

$$\mathcal{H}^{(I)}[\eta] = \frac{1}{2} \sum_j \left[\Pi_j^2 + \left\{ \Phi_j - \Phi_{j+1} \right\}^2 + \Lambda a^2(\eta) \Phi_j^2 \right] \quad ; \quad \eta = \frac{\tilde{\eta}}{\tilde{d}} \quad ; \quad \Lambda = \tilde{d}^2 \tilde{m}_f^2, \quad (80)$$

where we have now shifted to a Hamiltonian that is fully described by dimensionless conformal time η and dimensionless field mass Λ . When we follow a similar procedure to obtain the Hamiltonian in (dimensionless) cosmic time, we obtain:

$$\mathcal{H}^{(II)}[t] = \frac{1}{2a(t)} \sum_j \left[\Pi_j^2 + \left\{ \Phi_j - \Phi_{j+1} \right\}^2 + \Lambda a^2(t) \Phi_j^2 \right] \quad ; \quad t = \frac{\tilde{t}}{\tilde{d}} \quad ; \quad \Lambda = \tilde{d}^2 \tilde{m}_f^2, \quad (81)$$

We indeed see that the two Hamiltonians are connected the same way as in (53):

$$\mathcal{H}^{(II)}[t] = \frac{\mathcal{H}^{(I)}[\eta(t)]}{a(\eta(t))} \quad (82)$$

Following the same procedure as in Section III, we finally get:

$$\mathcal{H}^{(II)}[t] = \frac{1}{2} \sum_j \left[\pi_j^2 + \frac{(\varphi_j - \varphi_{j+1})^2}{a^2(t)} + \Omega^2(t) \varphi_j^2 \right] \quad ; \quad \Omega^2(t) = \Lambda + \frac{1}{4} \left(\frac{\dot{a}}{a} \right)^2 - \frac{\ddot{a}}{2a} \quad (83)$$

It should be noted that on going from conformal-time to cosmic-time Hamiltonian, the regularization that places field amplitudes along the comoving lattice $\tilde{x} = j\tilde{d}$ is preserved. Canonical transformations meanwhile act on the regularized field amplitudes, keeping the lattice structure intact. Therefore any bipartition in the real-space also carries over from $\mathcal{H}^{(I)}(\eta)$ to $\mathcal{H}^{(II)}(t)$, and the spatial entanglement can be directly compared for both representations.

The normal modes spectrum for $\mathcal{H}^{(II)}(t)$ is given below [45, 76, 77]:

$$\omega_j^2(t) = \Omega^2(t) + \frac{4}{a^2} f_j^2 \quad ; \quad f_j = \begin{cases} \sin \left[\frac{j\pi}{2(N+1)} \right] & \text{Dirichlet} \\ \sin \left[\frac{(j-1)\pi}{2N} \right] & \text{Neumann} \end{cases} \quad (84)$$

In the massless limit $\Lambda \rightarrow 0$, and in terms of dimensionless Hubble parameter H , the normal modes become:

$$\omega_j^2(t) = \frac{4}{a^2} f_j^2 - \frac{1}{4} \left(H^2 + 2\dot{H} \right) \quad ; \quad H = \frac{\dot{a}(t)}{a(t)} = \tilde{H}\tilde{d} \quad (85)$$

In the thermodynamic limit $N \rightarrow \infty$, we may further rewrite the normal mode equation in terms of (dimensionless) co-moving momentum k_j as follows:

$$4a^2\omega_j^2 \sim k_j^2 - a^2H^2 - 2a^2\dot{H} \quad ; \quad k_j = \frac{2\pi j}{N} = \tilde{k}_j\tilde{d}, \quad (86)$$

where we see that the normal mode spectrum maps to Fourier modes (for a lattice this spectrum is just the discrete fourier transform [78]). Shifting from co-moving to physical normal modes ($\bar{\omega}_j = a\omega_j$) and physical momenta ($\bar{k}_j = k_j/a$), we get:

$$4\bar{\omega}_j^2 \sim \bar{k}_j^2 - H^2 - 2\dot{H} \quad (87)$$

The normal mode $\bar{\omega}_j$ therefore corresponds to a momentum-mode \bar{k}_j that is either sub-Hubble ($k_j > H$) or super-Hubble ($k_j < H$), whereas its *stability* depends further on \dot{H} . We see that the inversion/squeezing of super-Hubble modes in general are amplified by an accelerated expansion ($\dot{H} > 0$) and suppressed by a decelerated expansion ($\dot{H} < 0$). On the other hand, the stability of sub-Hubble modes is enhanced by a decelerated expansion ($\dot{H} < 0$) and worsened by an accelerated expansion ($\dot{H} > 0$).

In the case of $(1+1)$ -dimensions, we may easily resolve the problem of quantum-classical transition via the connection formulas developed in Section III. In the massless limit $\Lambda \rightarrow 0$, we observe that the Hamiltonian $H^{(I)}$ is time(η)-independent. As a result of this, the conformal-time scaling parameters are trivially fixed:

$$B_j(\eta) = 1 \quad ; \quad B'_j(\eta) = 0 \quad (88)$$

Using (65), we see that:

$$\frac{\omega(t_0)}{b^2(t)} = \frac{\Omega(\eta_0)}{a(t)} \quad ; \quad \frac{\dot{b}(t)}{b(t)} = \frac{\dot{a}(t)}{2a(t)} \quad (89)$$

Since the entanglement entropy is a symplectic invariant, cosmic-time Hamiltonian must also result in constant entropies. However, log classicality depends on the choice of conjugate variables, i.e., in this case, the time co-ordinate employed. In any case, however, since entanglement entropy remains a constant throughout, massless fluctuations *never* undergo a quantum-classical transition in $(1+1)$ -dimensions, regardless of squeezing or the choice of conjugate variables. We confirm this through numerical simulations of the cosmic-time Hamiltonian, which is explicitly time-dependent even in the massless case. For this demonstrative exercise, we consider two types of time-dependent background: (i) $a(t) \propto 1 + A \tanh(Qt)$, where A and Q are constants. This describes a universe that smoothly

expands by a finite factor over its entire evolution from asymptotic past to future, and (ii) $a(t) \propto e^{Ht}$, which corresponds to a De-Sitter universe.

A. Tanh Expansion

We first consider a simple evolution used for studying particle-production in an expanding background, with an asymptotic past and future where the in- and out- vacua are well-defined [79]:

$$a(t) = \frac{1}{2} [\{a_1 + a_0\} + \{a_1 - a_0\} \tanh(Qt)] = \frac{a_0 + a_1 e^{2Qt}}{1 + e^{2Qt}} \quad (90)$$

where a_0 and a_1 are the respective initial and final values of the evolving scale factor and Q^{-1} is the time-scale of quench. Upon evolving from $t_0 \rightarrow -\infty$, the scaling parameter for all the modes can be obtained from (65) as follows:

$$b_j(t) = \sqrt{\frac{1 + \frac{a_1}{a_0} e^{2Qt}}{1 + e^{2Qt}}} \quad (91)$$

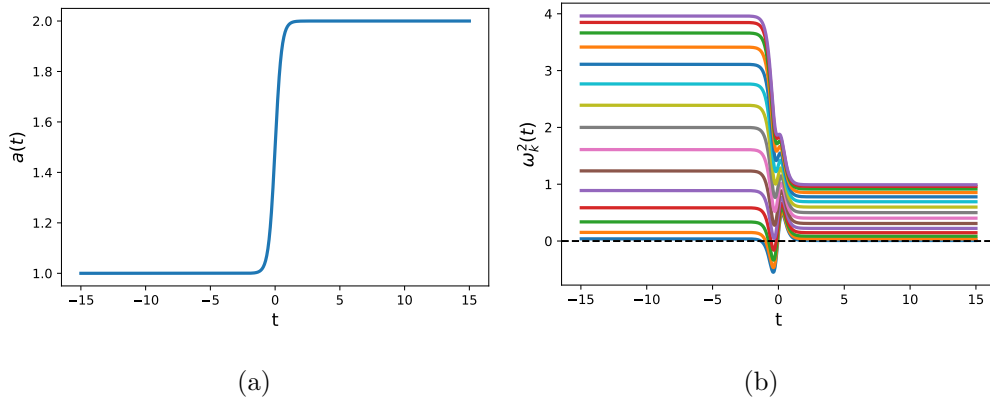


FIG. 2: Evolution of (a) scale factor $a(t)$ and the corresponding (b) normal mode spectrum in $(1+1)$ -dimensions. It can be seen that some normal modes are briefly inverted during the expansion. Here, $N = 15$, $a_0 = 1$, $a_1 = 2$ and $Q = 2$.

From Fig. 2, we see that some of the modes undergo a brief inversion during the expansion, signified by the period in which $\omega_k^2(t) < 0$. While it has no effect on entanglement entropy (symplectic invariance ensures that it stays constant regardless of the choice of conjugate variables), it translates to a brief squeezing of the reduced Wigner function and eventual

stabilization, clearly captured by the log classicality plot (LC vs t) in Fig. 3. This short-lived squeezing is a byproduct of choosing conjugate variables in the cosmic-time Hamiltonian, whereas the same is completely absent ($LC = 0$) upon considering conformal-time conjugate variables. Both choices, therefore, fail to satisfy the two-fold classicality criteria.

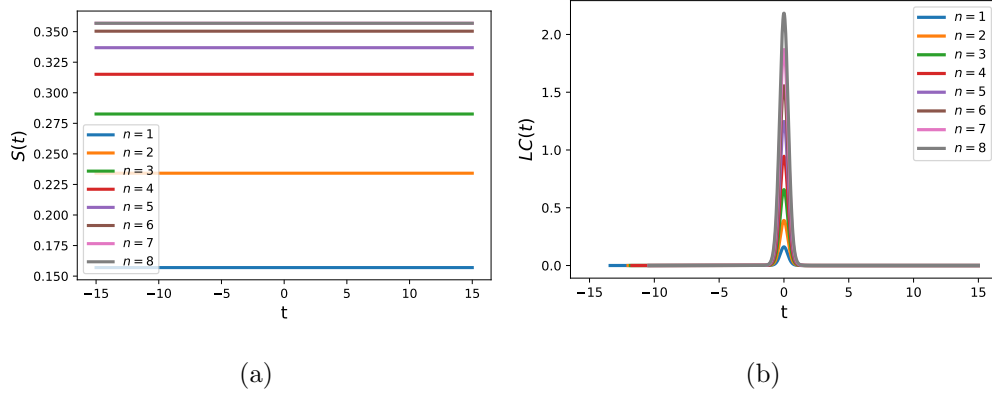


FIG. 3: Evolution of (a) entanglement entropy $S(t)$ and (b) log classicality $LC(t)$ for a Tanh-quench in $(1+1)$ -dimensions. Here, $N = 15$ and $H = 0.5$.

B. De-Sitter Expansion

The scale factor during de-Sitter expansion takes the following form:

$$a(t) = a_0 e^{H(t-t_0)}, \quad (92)$$

where a_0 is the initial value of the scale factor at $t = t_0$, and H is the Hubble constant. Substituting this into (81), we obtain a Hamiltonian that describes a chain of Caldirola-Kanai oscillators [80, 81] with nearest-neighbour coupling, and therefore the results we outline here are in turn relevant to understanding dissipative systems. The classical solution for each mode in this case can be obtained by solving:

$$y_j''(t) + \omega_j^2(t)y_j(t) = 0 \quad (93)$$

where the normal-mode spectrum is given by:

$$\omega_j^2(t) = -\frac{H^2}{4} + \frac{4}{a_0^2} f_j^2 e^{-2H(t-t_0)} \quad (94)$$

We obtain the independent solutions to be $y_j(t)$ and $y_j^*(t)$, where:

$$y_j(t) = \exp\left\{\frac{1}{2}Ht + i\frac{2f_j}{a_0H}e^{-Ht}\right\} \quad ; \quad W[y_j, y_j^*] = 4if_j. \quad (95)$$

Using (59), we obtain the scaling parameters as follows:

$$b_j^2(t) = \left[e^{-Ht_0} - \frac{a_0H}{4f_j} \sin\left\{\frac{4f_j(e^{-Ht_0} - e^{-Ht})}{a_0H}\right\} \right] e^{Ht} \quad (96)$$

It should be noted that the above solution for each j -mode is only valid if $a_0H < 4f_j$, which along with (94) tells us that no mode can be inverted at the beginning of the evolution $t = t_0$.

In the long-time limit, the scaling parameter takes a similar form as (30):

$$b_j \sim c_j e^{\frac{H(t-t_0)}{2}} \quad ; \quad c_j = \sqrt{1 - \frac{a_0He^{Ht_0}}{4f_j} \sin\left(\frac{4f_je^{-Ht_0}}{a_0H}\right)} \quad (97)$$

The key thing to note here is that all the k -modes that cross the horizon will have the exact same exponential growth factor ($\sim H/2$) for their respective scaling parameters $b_j(t)$. This eventually results in the saturation of entropy growth (Appendix A), the time-scale (t_{sat}) for which is given by the inversion time for the mode with the largest index, i.e., $j = N$. For large N , this time-scale can be obtained from (94):

$$t_{sat} \sim t_0 + \frac{1}{H} \log \frac{4}{a_0H} \quad (98)$$

However, if we consider the beginning of the evolution to be at $t_0 = -\infty$, the connections and the conditions in (89) are satisfied, thereby matching the vacua in both cosmic-time and conformal-time and greatly simplifying the problem. The entanglement entropy therefore saturates instantly ($t_{sat} \rightarrow -\infty$) and it remains time-independent throughout the evolution, consistent with the results for the time-independent form conformal-time Hamiltonian. However, the classicality parameter picks up a non-trivial behaviour upon choosing cosmic-time conjugate variables.

From Fig. 4, we see that all the normal modes for a de-Sitter expansion in cosmic-time conjugate variables eventually get inverted, and furthermore, they converge asymptotically to the same value, i.e., it exhibits an ungapped inverted mode spectrum as $t \rightarrow \infty$. In Fig. 5, the runaway squeezing of the reduced Wigner function translates to a linear growth of log classicality once the first mode becomes inverted (i.e., it has crossed the horizon), and its slope is found to saturate once all the modes have become inverted. The entanglement

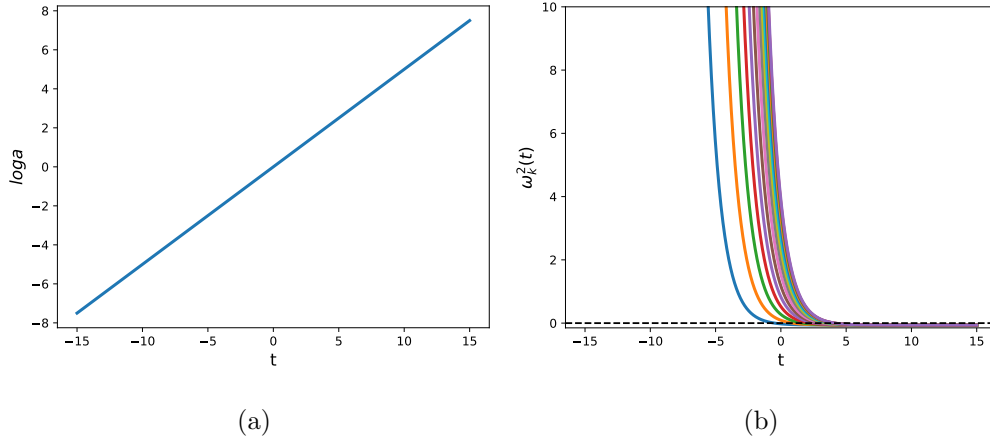


FIG. 4: Evolution of (a) scale factor $a(t)$ and (b) Normal mode spectrum for de-Sitter expansion in $(1+1)$ -dimensions. Here, $N = 15$ and $H = 0.5$.

entropy, despite mode inversion, stays constant. The overall behaviour for any subsystem size in cosmic-time conjugate variables can be summarized below:

$$S(t) = \text{const} \quad ; \quad \lim_{t \rightarrow \infty} LC(t) \propto Ht \quad (99)$$

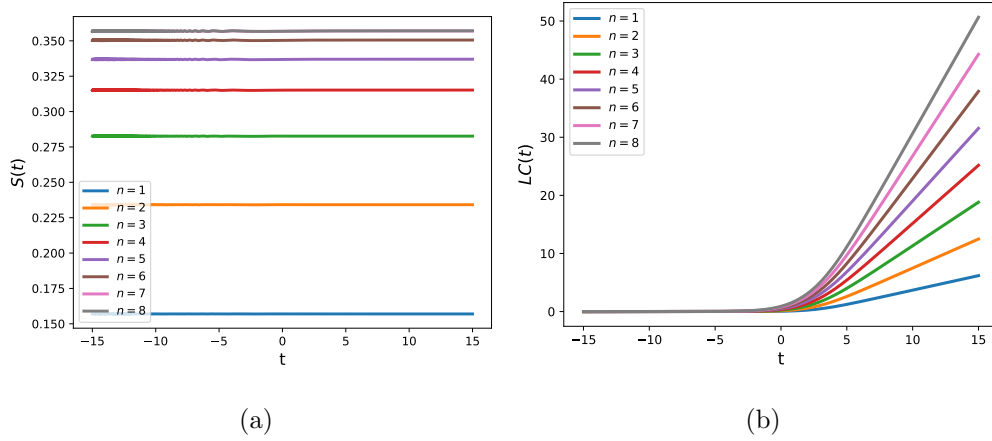


FIG. 5: Evolution of (a) entanglement entropy $S(t)$ and (b) Log classicality $LC(t)$ for de-Sitter expansion in $(1+1)$ -dimensions. Here, $N = 15$ and $H = 0.5$.

While the Tanh and de-Sitter models have proved useful in understanding the effects of mode-inversion and squeezing of the Wigner function for large subsystem-sizes, the

time-independent behaviour of entanglement entropy effectively rules out any occurrence of quantum-classical transition in $(1+1)$ -dimensions. This is also a perfect example of — i) how squeezing by itself does not imply classicality, echoing the ungapped inverted mode scenario in the CHO (Table I), and ii) how inverted mode instabilities do not always generate a linear growth in entanglement entropy, in contrast with recent works [45, 67]. We now turn our attention to $(3+1)$ -dimensions in the next section, and apply the classicality criteria for fluctuations propagating in an expanding background.

V. EARLY-UNIVERSE FLUCTUATIONS IN $(3+1)$ -D

In this Section, we apply the classicality criteria for fluctuations propagating in $(3+1)$ -dimensions. The unperturbed expanding background in $(3+1)$ -dimensions in co-moving coordinates $(\tilde{r}, \theta, \phi)$ clocked by cosmic time (\tilde{t}) or conformal time $(\tilde{\eta})$ is described by:

$$ds^2 = d\tilde{t}^2 - a^2(\tilde{t})(d\tilde{r}^2 + \tilde{r}^2 d\Omega^2) = a^2(\tilde{\eta}) [d\tilde{\eta}^2 - (d\tilde{r}^2 + \tilde{r}^2 d\Omega^2)] \quad ; \quad d\tilde{t} = a(\tilde{\eta})d\tilde{\eta}, \quad (100)$$

where $d\Omega^2 = d\theta^2 + \sin^2 \theta d\phi^2$. In terms of the conformal-time, the Lagrangian for a massive test scalar field in an expanding background is given by:

$$L = \frac{a^2(\tilde{\eta})}{2} \int d\tilde{r} d\theta d\phi \tilde{r}^2 \sin \theta \left[\tilde{\Phi}'^2 - (\partial_{\tilde{r}} \tilde{\Phi})^2 - \frac{1}{\tilde{r}^2} (\partial_{\theta} \tilde{\Phi})^2 - \frac{1}{\tilde{r}^2 \sin^2 \theta} (\partial_{\phi} \tilde{\Phi})^2 - a^2(\tilde{\eta}) \tilde{m}_f^2 \tilde{\Phi}^2 \right] \quad (101)$$

In the massless limit, the above system equivalently describes the leading (linear) order scalar perturbations of the background metric. We may employ spherical decomposition to reduce the system to an effective $(1+1)$ -dimensional system [35, 42]:

$$\tilde{\Pi} = \frac{1}{\tilde{r}} \sum_{lm} \tilde{\Pi}_{lm}(\tilde{r}) Z_{lm}(\theta, \phi) \quad ; \quad \tilde{\Phi} = \frac{1}{\tilde{r}} \sum_{lm} \tilde{\Phi}_{lm}(\tilde{r}) Z_{lm}(\theta, \phi) \quad (102)$$

Upon further obtaining the canonical momentum $\tilde{\Pi}_{lm} = \partial_{\tilde{\Phi}'_{lm}} L$, and discretizing the system as $\tilde{r} = j\tilde{d}$, we get:

$$\mathcal{H}[\tilde{\eta}] = \frac{1}{2\tilde{d}} \sum_{lmj} \left[\frac{\tilde{\Pi}_{lmj}^2}{a^2(\tilde{\eta})} + a^2(\tilde{\eta}) \left(j + \frac{1}{2} \right)^2 \left\{ \frac{\tilde{\Phi}_{lmj}}{j} - \frac{\tilde{\Phi}_{lm,j+1}}{j+1} \right\}^2 + \tilde{d}^2 \tilde{m}_f^2 a^4(\tilde{\eta}) \tilde{\Phi}_{lmj}^2 \right] = \sum_{lm} \frac{\mathcal{H}_{lm}^{(I)}}{\tilde{d}} \quad (103)$$

The UV-cutoff \tilde{d} can be absorbed and the Hamiltonian can be rewritten in terms of dimensionless parameters as follows [42]:

$$\mathcal{H}_{lm}^{(I)}[\eta] = \frac{1}{2} \sum_{lmj} \left[\Pi_{lmj}^2 + \left(j + \frac{1}{2} \right)^2 \left\{ \frac{\Phi_{lmj}}{j} - \frac{\Phi_{lm,j+1}}{j+1} \right\}^2 + \left(\Lambda a^2(\tilde{\eta}) - \frac{a''(\eta)}{a(\eta)} + \frac{l(l+1)}{j^2} \right) \Phi_{lmj}^2 \right] \quad (104)$$

where we have defined dimensionless conformal time $\eta = \tilde{d}^{-1} \tilde{\eta}$ and dimensionless field mass $\Lambda = \tilde{d}^2 \tilde{m}_f^2$. Unlike the $(1+1)$ -D case, we see that the massless conformal-time Hamiltonian has an explicit time(η)-dependence in $(3+1) - D$ case, thereby leading to non-trivial dynamics in entanglement entropy and log classicality. When we follow a similar procedure to obtain the Hamiltonian in cosmic time, we see that the following relation holds as laid out in Section III:

$$\mathcal{H}_{lm}^{(II)}[t] = \frac{\mathcal{H}_{lm}^{(I)}[\eta]}{a(\eta(t))}. \quad (105)$$

We therefore obtain the following Hamiltonian in terms of (dimensionless) cosmic time:

$$\mathcal{H}_{lm}^{(II)}[t] = \frac{1}{2} \sum_{lmj} \left[\Pi_{lmj}^2 + \frac{1}{a^2(t)} \left(j + \frac{1}{2} \right)^2 \left\{ \frac{\Phi_{lmj}}{j} - \frac{\Phi_{lm,j+1}}{j+1} \right\}^2 + \Omega_{lmj}^2(t) \Phi_{lmj}^2 \right] \quad ; \quad t = \frac{\tilde{t}}{\tilde{d}}, \quad (106)$$

where,

$$\Omega_{lmj}^2(t) = \Lambda + \frac{l(l+1)}{j^2 a^2(t)} - \frac{3}{4} \left(\frac{\dot{a}(t)}{a(t)} \right)^2 - \frac{3\ddot{a}(t)}{2a(t)} \quad (107)$$

Unlike in $(1+1)$ -dimensions, the coupling matrix in $(3+1)$ -dimensions is not a Toeplitz matrix, as a result of which an exact analytic expression for the normal mode spectrum cannot be obtained [42]. However, using the insights from the normal mode spectrum obtained in Section IV and comparing it with the effective frequencies in (107), we can infer that mode inversion is facilitated in cases of accelerated expansion, i.e., $\ddot{a} > 0$. The extra input that we get here is that the angular momentum term, whose contribution is maximum at early times, *counters* mode-inversion. The low- l modes are the first to get inverted, whereas large- l modes follow suit at later times. We sum up the angular-momentum contributions, which are expected to converge as $l \rightarrow \infty$ for $(3+1)$ -dimensions [35], as follows:

$$S(t) = \sum_l (2l+1) S_l(t) \quad ; \quad LC(t) = \sum_l (2l+1) LC_l(t) \quad (108)$$

For the rest of this section, we rely on numerics to see how various expansion models fare in the classicality test developed in Section II.

A. Tanh Evolution

For the same quench function used in (90), we see from Fig. 6 that the entanglement entropy has a stable oscillatory behaviour throughout whereas log classicality temporarily peaks when the expansion kicks in. This is quite similar to the behaviour observed in $(1+1)$ –dimensions, except that the entanglement entropy is no longer a constant. As a result, such an expansion does not satisfy the classicality criteria either in $(1+1)$ –dimensions or in $(3+1)$ –dimensions.

The above results indicate that during a Tanh expansion in $(3+1)$ –dimensions, the momentum modes of discretized linear fluctuations briefly become inverted when they cross the Hubble radius, and stabilize when they reenter. Such an evolution causes *spatial* bipartitions of fluctuations in the co-moving frame to maintain its coherence (S has stable oscillatory behaviour) and exhibit a high-degree of classical correlations (sharp peak in LC) during this brief inversion. Upon reentering, the fluctuations recover from this brief buildup of classical correlations in the system, which can also be accompanied by an increase in $R_{(x,p)}$, the relative strength (25) of quantum to classical contributions in observables. Therefore, in both $(1+1)$ – and $(3+1)$ –dimensions, the real-space bipartitions of fluctuations in the comoving frame regain their quantumness as the scale factor of expansion relaxes to a final value.

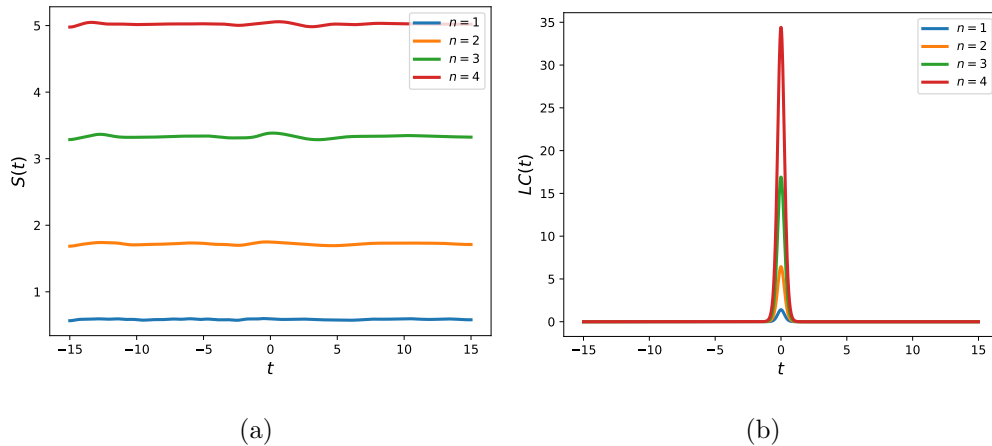


FIG. 6: Evolution of (a) entanglement entropy $S(t)$ and (b) Log classicality $LC(t)$ for Tanh expansion in $(3+1)$ –dimensions. Here, $a_0 = 1$, $a_1 = 2$, $Q = 2$, $N = 5$ and we count up to $l = 200$.

B. de-Sitter Expansion

During a de-Sitter expansion (92) in $(3+1)$ –dimensions, we see from Fig. 7 that both the entanglement entropy and log classicality of all subsystem sizes exhibit unbounded growth in time, thereby fulfilling the classicality criteria at late-times. This is in stark contrast with the behaviour observed in $(1+1)$ –dimensions, where the entanglement entropy remained constant, thereby failing the classicality criteria at late-times. The fluctuations therefore undergo a quantum-classical transition in a de-Sitter background in $(3+1)$ –dimensions, but not in $(1+1)$ –dimensions.

Physically, this implies that during a de-Sitter expansion in $(3+1)$ –dimensions, the momentum modes of discretized linear fluctuations become inverted as they cross the Hubble radius. This inversion in turn causes *spatial* bipartitions of fluctuations in the co-moving frame to both quickly decohere ($S \rightarrow \infty$) and also exhibit a high-degree of classical correlations ($LC \rightarrow \infty$). The Gaussian nature of fluctuations further enables Hermitian observables of the form in (24) to be fully described in terms of two-point functions. However, non-trivial quantum signatures in such observables are rapidly suppressed in the classicality limit as discussed in (25). As a result, at late-times, real-space bipartitions of fluctuations in the co-moving frame are essentially described by classical statistical ensembles, with their phase-space distribution sharply peaking about classical trajectories. This also implies that at late-times, it is nearly impossible to distinguish whether these fluctuations were of quantum or classical origin without high-precision observations.

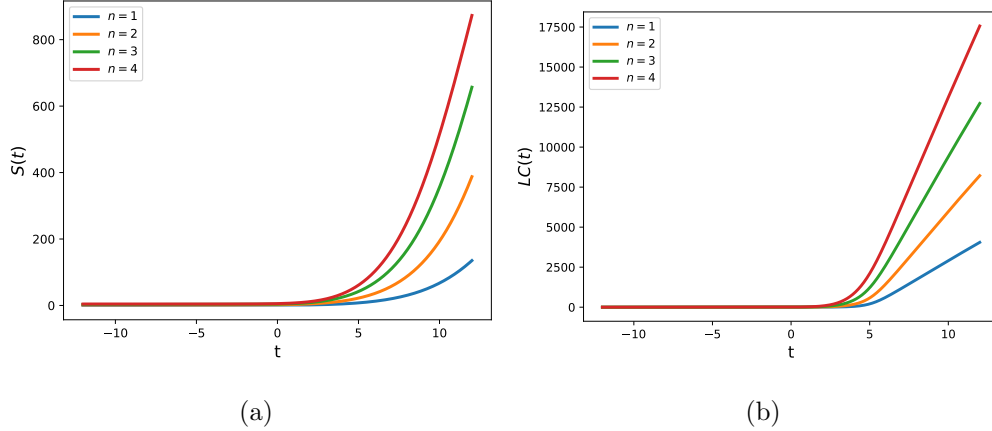


FIG. 7: Evolution of (a) entanglement entropy $S(t)$ and (b) Log classicality $LC(t)$ for de-Sitter expansion in $(3+1)$ -dimensions. Here, $N = 5$, $H = 0.5$ and we count up to $l = 20$.

VI. CONCLUSIONS AND DISCUSSIONS

In this work, our primary focus is to understand the quantum-to-classical transition of entangled quadratic systems with spatial degrees of freedom. Our investigation involved three distinct signatures of classical behavior: i) decoherence as a measure of how well the system can be described by a classical statistical ensemble, ii) runaway squeezing of the Wigner function about classical phase-space trajectories, and iii) rapid suppression of non-commutativity in observables. We developed the necessary tools in Section II to extract and measure these signatures in terms of entanglement entropy $S(t)$, log classicality $LC(t)$, and relative strength $R_{(x,p)}$ from a multi-mode Gaussian state.

We obtained a simple geometric picture of the interplay between these signatures through the stability analysis of the reduced Wigner function of the subsystem, as illustrated in Fig. 1. The results, summarized in Table I, reveals that the presence of instabilities arising from a gapped inverted mode spectrum in the system leads to the emergence of all three classicality signatures in the CHO (quadratic system). On the other hand, other stability regimes exhibited only partial or no indications of classical behavior.

Furthermore, in Section III, we investigated the dependence of these signatures on conjugate variables by exploring canonical transformations connecting conformal time (η) to cosmic time (t) Hamiltonians. While entanglement entropy is a symplectic invariant, the

other two measures showed explicit dependence on the choice of conjugate variables. This observation suggests that although decoherence is the strongest and most reliable condition for classical behavior to manifest in quantum systems [22], certain choices of conjugate variables could lead to a higher degree of classical correlations and faster suppression of quantum signatures during subsystem evolution.

Next, in Section IV, we analyzed linear fluctuations of an expanding background in $(1+1)$ dimensions. We found that a quantum-to-classical transition did not occur as the dynamics preempted decoherence. This was demonstrated by considering two different scale factors of expansion: i) a Tanh expansion with fixed values at asymptotic past and future, and ii) an exponentially growing scale factor corresponding to a de-Sitter expansion. In Section V, we extended the analysis to $(3+1)$ –dimensions and showed that the background fluctuations of a Tanh expansion eventually recovered their quantum nature, whereas a de-Sitter expansion underwent a quantum-to-classical transition.

Throughout, we discovered that the inversion of normal modes in momentum-space acted as a common trigger for the emergence of classical behavior. While this inversion had limited impact on the momentum space of quadratic systems, it significantly affected the entangled degrees of freedom in real-space. For a flat background in $(1+1)$ dimensions, recent studies have revealed that: i) the entanglement entropy “classicalizes” i.e., it mimics the statistical entropy of classically chaotic systems via a linear growth, wherein the growth rate is given by the sum of all positive Lyapunov exponents [45, 67, 82, 83], ii) the leading order behavior of entanglement entropy asymptotically converges with other correlation measures, such as fidelity, Loschmidt echo, and circuit complexity of the entire system [45], and iii) entanglement entropy asymptotically transitions from an area-law to a volume-law with subsystem size, thereby mimicking thermodynamic entropy [45, 84, 85]. In addition to our analysis, these effects further signal the emergence of both classical *and* possible thermodynamic behaviour in the real-space from quantum foundations. However, the generalization of these properties to higher dimensions is subject of future work and will be addressed elsewhere using the tools developed here.

Our analysis may further provide the tools necessary to distinguish between cosmological models, such as those with similar observable power spectra, as has been the subject of recent investigations [86]. Of particular interest is using these measures to distinguish inflation from bounce, which is currently under investigation. Lastly, a generalization of our real-space

approach to account for higher-order curvature perturbations is an outstanding problem we hope to address in future works. Resolving this can filter out the spatial effects exclusively arising from non-Gaussianity in the context of the quantum-to-classical transition problem while also laying out potential new ways of obtaining direct observational evidence for the quantum origin of CMB fluctuations.

ACKNOWLEDGMENTS

The authors thank Suddhasattwa Brahma, Ashu Kushwaha, Orlando Luongo, Amaury Micheli, Abhishek Naskar and Vincent Vennin for useful discussions. SMC is supported by Prime Minister's Research Fellowship offered by the Ministry of Education, Govt. of India. The work is supported by the SERB Core Research grant.

Appendix A: Conditions for purity saturation

The purity of CHO has the following form:

$$\delta_{QD}(t) = \sqrt{\frac{4K_+K_-}{(K_+ + K_-)^2 + (L_+ - L_-)^2}} \quad ; \quad K_{\pm} = \frac{\omega_{\pm}(t_0)}{b_{\pm}^2} \quad ; \quad L_{\pm} = \frac{\dot{b}_{\pm}}{b_{\pm}} \quad (\text{A1})$$

Let us now rewrite $b_-(t) = f(t)b_+(t)$:

$$\delta_{QD}(t) = \sqrt{\frac{4\omega_+(t_0)\omega_-(t_0)}{(f\omega_+(t_0) + f^{-1}\omega_-(t_0))^2 + f\dot{b}_+^4}} \xrightarrow{f \rightarrow 0} \frac{\sqrt{4\omega_+(t_0)\omega_-(t_0)}}{f\omega_+(t_0) + f^{-1}\omega_-(t_0)}, \quad (\text{A2})$$

where we see that the evolution of purity (and thereby entanglement entropy) saturates in regimes where the Ermakov solutions $b_{\pm}(t)$ have the same time-evolution ($\dot{f} = 0$) upto a proportionality constant (f).

Appendix B: Entanglement entropy of CHO

Like in the case of time-independent CHO [35, 87], to evaluate the entanglement entropy, we must first calculate the eigenvalues of the reduced density matrix (RDM) of the system [35, 66] by solving the following integral equation [35, 87]:

$$\int dx'_2 \rho_2(x_2, x'_2) f_n(x'_2) = p_n f_n(x_2). \quad (\text{B1})$$

The solution for the above integral equation is [66]:

$$\begin{aligned}
f_n(x) &= \frac{1}{\sqrt{2^n n!}} \left(\frac{\epsilon}{\pi} \right)^{1/4} H_n(\sqrt{\epsilon} x) \exp \left\{ -(\epsilon + i\delta) \frac{x^2}{2} \right\} \\
\epsilon &= \sqrt{\Gamma_1^2 - \Gamma_2^2} \\
p_n &= (1 - \xi(t)) \xi^n(t) \\
\xi(t) &= \frac{\Gamma_2}{\Gamma_1 + \epsilon} = \frac{\sqrt{\left(\frac{\omega_+(t_0)}{b_+^2(t)} + \frac{\omega_-(t_0)}{b_-^2(t)} \right)^2 + \left(\frac{\dot{b}_+(t)}{b_+(t)} - \frac{\dot{b}_-(t)}{b_-(t)} \right)^2} - 2\sqrt{\frac{\omega_+(t_0)\omega_-(t_0)}{b_+(t)b_-(t)}}}{\sqrt{\left(\frac{\omega_+(t_0)}{b_+^2(t)} + \frac{\omega_-(t_0)}{b_-^2(t)} \right)^2 + \left(\frac{\dot{b}_+(t)}{b_+(t)} - \frac{\dot{b}_-(t)}{b_-(t)} \right)^2} + 2\sqrt{\frac{\omega_+(t_0)\omega_-(t_0)}{b_+(t)b_-(t)}}}
\end{aligned} \tag{B2}$$

The entanglement entropy is calculated as follows:

$$S(t) = - \sum_n p_n \log p_n = - \log [1 - \xi(t)] - \frac{\xi(t)}{1 - \xi(t)} \log \xi(t), \tag{B3}$$

Appendix C: Entanglement entropy of N-HO with time-dependent frequencies

Consider the following Hamiltonian [45]:

$$H = \frac{1}{2} \sum_{i=1}^N p_i^2 + \frac{1}{2} \sum_{i,j=1}^N K_{ij} x_i x_j, \tag{C1}$$

The coupling matrix (K_{ij}) here has time-dependent entries and captures all the necessary information about correlations in the system. The initial values of normal modes, labelled as $\{\omega_i(t_0)\}$, are the eigenvalues of $K^{1/2}(t_0)$. The ground state wave-function here is given by [45]:

$$\Psi_{\text{GS}}(\tilde{X}, t) = \left(\prod_{n=1}^N \frac{\omega_n(t_0)}{\pi b_n^2(t)} \right)^{1/4} \exp \left\{ -\frac{1}{2} \tilde{X}^T (\Omega_D^{1/2} - i Z_D) \tilde{X} - \frac{i}{2} \sum_{n=1}^N \omega_n(t_0) \tau_n \right\}, \tag{C2}$$

where $\tilde{X} = MX$ is the normal mode co-ordinate system that diagonalizes the Hamiltonian. We also see that Ω_D and Z_D are diagonal matrices whose entries are given below:

$$(\Omega_D)_{nn} = \frac{\omega_n(t_0)}{b_n^2(t)} \quad ; \quad (Z_D)_{nn} = \frac{\dot{b}_n(t)}{b_n(t)} \tag{C3}$$

In the physical co-ordinates, the wave-function is entangled, taking the following form:

$$\Psi_{\text{GS}}(X, t) = \left(\prod_{n=1}^N \frac{\omega_n(t_0)}{\pi b_n^2(t)} \right)^{1/4} \exp \left\{ -\frac{1}{2} [X^T (\Omega - i Z) X] - \frac{i}{2} \sum_{n=1}^N \omega_n(t_0) \tau_n \right\}, \tag{C4}$$

where $Z = MZ_DM^T$ and $\Omega = M\Omega_DM^T$. In order to trace out some m degrees of freedom from the system, let us first rewrite the following matrices:

$$\Omega = \begin{bmatrix} (A)_{m \times m} & (B)_{m \times N-m} \\ (B^T)_{N-m \times m} & (C)_{N-m \times N-m} \end{bmatrix} \quad ; \quad Z = \begin{bmatrix} (Z_A)_{m \times m} & (Z_B)_{m \times N-m} \\ (Z_B^T)_{N-m \times m} & (Z_C)_{N-m \times N-m} \end{bmatrix} \quad (\text{C5})$$

To calculate entanglement entropy, we first obtain the reduced density matrix as follows:

$$\rho_{out} = \sqrt{\frac{\det\{\Omega/\pi\}}{\det\{A/\pi\}}} \exp\left\{-\frac{1}{2}X'_{out}(\Gamma_1 + i\Gamma_3)X'_{out} - \frac{1}{2}X_{out}^T(\Gamma_1 - i\Gamma_3)X_{out} + X_{out}^T\Gamma_2X'_{out}\right\} \quad (\text{C6})$$

where we see that:

$$\begin{aligned} \Gamma_1 &= C - \frac{1}{2}B^TA^{-1}B + \frac{1}{2}Z_B^TA^{-1}Z_B \\ \Gamma_2 &= \frac{1}{2}B^TA^{-1}B + \frac{1}{2}Z_B^TA^{-1}Z_B \\ \Gamma_3 &= Z_C - Z_B^TA^{-1}B \end{aligned} \quad (\text{C7})$$

Now we perform a series of diagonalizations to simplify the RDM further. Let V be a diagonalizing matrix for Γ_1 such that $\Gamma_1 = V^T\Gamma_{1D}V$ and $\Gamma = \Gamma_{1D}^{-1/2}V\Gamma_2V^T\Gamma_{1D}^{-1/2}$. Let W diagonalize Γ such that

$$\Gamma = W^T\Gamma_DW \quad \tilde{\Gamma}_3 = W\Gamma_{1D}^{-1/2}V\Gamma_3V^T\Gamma_{1D}^{-1/2}W^T. \quad (\text{C8})$$

In the new co-ordinates $Y = W\Gamma_{1D}^{1/2}VX_{out} = \{y_j\}$, the RDM can hence be rewritten as:

$$\rho_{out} = \frac{1}{\pi^{N-m}} \exp\left\{\frac{i}{2} \left[Y^T\tilde{\Gamma}_3Y - Y'^T\tilde{\Gamma}_3Y' \right]\right\} \prod_{j=m+1}^N \sqrt{1-\Gamma_j} \exp\left\{-\frac{1}{2}(y_j^2 + y_j'^2) + \Gamma_j y_j y_j'\right\}, \quad (\text{C9})$$

where Γ_j are the eigenvalues of Γ . The integral eigenvalue equation for RDM will therefore have the following solution:

$$\begin{aligned} f_n(Y, t) &= \left(\prod_{j=m+1}^N H_n(\epsilon^{1/2}y_j) \right) \exp\left\{-Y^T \left(\frac{\epsilon - i\tilde{\Gamma}_3}{2} \right) Y\right\} \\ p_n(t) &= \prod_{j=m+1}^N (1 - \xi_j(t)) \xi_j^n(t) \\ \xi_j(t) &= \frac{\Gamma_j}{1 + \sqrt{1 - \Gamma_j^2}} \end{aligned} \quad (\text{C10})$$

The entanglement entropy therefore accumulates contributions from each of the remaining degrees of freedom as $S = \sum_{j=m+1}^N S_j(t)$ where $S_j(t)$ has the familiar form [45]:

$$S_j(t) = -\log[1 - \xi_j(t)] - \frac{\xi_j(t)}{1 - \xi_j(t)} \log \xi_j(t) \quad (\text{C11})$$

-
- [1] J. J. Halliwell, *Phys. Rev. D* **39**, 2912 (1989).
 - [2] T. Padmanabhan, *Phys. Rev. D* **39**, 2924 (1989).
 - [3] V. Vedral, *Nature* **453**, 1004 (2008).
 - [4] J. Eisert, M. Cramer, and M. B. Plenio, *Rev. Mod. Phys.* **82**, 277 (2010).
 - [5] W. H. Zurek, *Phys. Rev. D* **26**, 1862 (1982).
 - [6] E. Joos and H. D. Zeh, *Z. Phys. B* **59**, 223 (1985).
 - [7] N. Aghanim *et al.* (Planck), *Astron. Astrophys.* **641**, A6 (2020), [Erratum: *Astron. Astrophys.* 652, C4 (2021)], [arXiv:1807.06209 \[astro-ph.CO\]](#).
 - [8] S. Alam *et al.* (eBOSS), *Phys. Rev. D* **103**, 083533 (2021), [arXiv:2007.08991 \[astro-ph.CO\]](#).
 - [9] V. F. Mukhanov and G. V. Chibisov, *Soviet Journal of Experimental and Theoretical Physics Letters* **33**, 532 (1981).
 - [10] A. H. Guth and S.-Y. Pi, *Phys. Rev. Lett.* **49**, 1110 (1982).
 - [11] S. Hawking, *Physics Letters B* **115**, 295 (1982).
 - [12] A. Starobinsky, *Physics Letters B* **117**, 175 (1982).
 - [13] J. M. Bardeen, P. J. Steinhardt, and M. S. Turner, *Phys. Rev. D* **28**, 679 (1983).
 - [14] R. Brandenberger, R. Laflamme, and M. Mijić, *Physica Scripta* **1991**, 265 (1991).
 - [15] D. Polarski and A. A. Starobinsky, *Classical and Quantum Gravity* **13**, 377 (1996).
 - [16] C. Kiefer, D. Polarski, and A. A. Starobinsky, *Int. J. Mod. Phys. D* **7**, 455 (1998), [arXiv:gr-qc/9802003](#).
 - [17] F. C. Lombardo and D. L. Nacir, *Phys. Rev. D* **72**, 063506 (2005).
 - [18] J. Martin and V. Vennin, *Phys. Rev. D* **93**, 023505 (2016).
 - [19] L. P. Grishchuk and Y. V. Sidorov, *Phys. Rev. D* **42**, 3413 (1990).
 - [20] A. Perez, H. Sahlmann, and D. Sudarsky, *Classical and Quantum Gravity* **23**, 2317 (2006).
 - [21] D. Sudarsky, *Int. J. Mod. Phys. D* **20**, 509 (2011), [arXiv:0906.0315 \[gr-qc\]](#).
 - [22] A. Ashtekar, A. Corichi, and A. Kesavan, *Phys. Rev. D* **102**, 023512 (2020).

- [23] V. Balasubramanian, M. B. McDermott, and M. Van Raamsdonk, *Phys. Rev. D* **86**, 045014 (2012).
- [24] S. S. Kumar and S. Shankaranarayanan, *Phys. Rev. D* **95**, 065023 (2017).
- [25] S. Brahma, O. Alaryani, and R. Brandenberger, *Phys. Rev. D* **102**, 043529 (2020).
- [26] S. Brahma, A. Berera, and J. Calderón-Figueroa, *Classical and Quantum Gravity* **39**, 245002 (2022).
- [27] J. Martin, A. Micheli, and V. Vennin, *JCAP* **04**, 051 (2022), [arXiv:2112.05037 \[quant-ph\]](#).
- [28] J. Martin, A. Micheli, and V. Vennin, *Europhysics Letters* **142**, 18001 (2023).
- [29] S. Brahma, A. Berera, and J. Calderón-Figueroa, *Journal of High Energy Physics* **2022**, 225 (2022).
- [30] C. Burgess, R. Holman, G. Kaplanek, J. Martin, and V. Vennin, *Journal of Cosmology and Astroparticle Physics* **2023**, 022 (2023).
- [31] J. Berjon, E. Okon, and D. Sudarsky, *Phys. Rev. D* **103**, 043521 (2021), [arXiv:2009.09999 \[gr-qc\]](#).
- [32] J.-T. Hsiang and B.-L. Hu, *Universe* **8**, 27 (2022), [arXiv:2112.04092 \[gr-qc\]](#).
- [33] I. Agullo, B. Bonga, P. Ribes-Metidieri, D. Kranas, and S. Nadal-Gisbert, (2023), [arXiv:2302.13742 \[quant-ph\]](#).
- [34] L. Bombelli, R. K. Koul, J. Lee, and R. D. Sorkin, *Phys. Rev. D* **34**, 373 (1986).
- [35] M. Srednicki, *Phys. Rev. Lett.* **71**, 666 (1993).
- [36] R. Müller and C. O. Lousto, *Phys. Rev. D* **52**, 4512 (1995).
- [37] P. Calabrese and J. Cardy, *Journal of Statistical Mechanics: Theory and Experiment* **2004**, P06002 (2004).
- [38] P. Calabrese and J. Cardy, *Journal of Physics A: Mathematical and Theoretical* **42**, 504005 (2009).
- [39] S. Mukohyama, M. Seriu, and H. Kodama, *Phys. Rev. D* **55**, 7666 (1997).
- [40] S. Mukohyama, M. Seriu, and H. Kodama, *Phys. Rev. D* **58**, 064001 (1998).
- [41] S. N. Solodukhin, *Living Rev. Rel.* **14**, 8 (2011), [arXiv:1104.3712 \[hep-th\]](#).
- [42] S. M. Chandran and S. Shankaranarayanan, *Phys. Rev. D* **102**, 125025 (2020).
- [43] J. Martin and V. Vennin, *Phys. Rev. D* **104**, 085012 (2021).
- [44] J. Martin and V. Vennin, *Journal of Cosmology and Astroparticle Physics* **2021**, 036 (2021).
- [45] S. M. Chandran and S. Shankaranarayanan, *Phys. Rev. D* **107**, 025003 (2023).

- [46] C. Viermann *et al.*, **Nature** **611**, 260 (2022), [arXiv:2202.10399 \[cond-mat.quant-gas\]](#).
- [47] N. Sánchez-Kuntz, A. Parra-López, M. Tolosa-Simeón, T. Haas, and S. Floerchinger, **Phys. Rev. D** **105**, 105020 (2022).
- [48] M. Tolosa-Simeón, A. Parra-López, N. Sánchez-Kuntz, T. Haas, C. Viermann, M. Sparn, N. Liebster, M. Hans, E. Kath, H. Strobel, M. K. Oberthaler, and S. Floerchinger, **Phys. Rev. A** **106**, 033313 (2022).
- [49] C. Marletto and V. Vedral, **Phys. Rev. Lett.** **119**, 240402 (2017), [arXiv:1707.06036 \[quant-ph\]](#).
- [50] S. Rijavec, M. Carlesso, A. Bassi, V. Vedral, and C. Marletto, **New J. Phys.** **23**, 043040 (2021), [arXiv:2012.06230 \[quant-ph\]](#).
- [51] S. Bose, A. Mazumdar, M. Schut, and M. Toroš, **Phys. Rev. D** **105**, 106028 (2022).
- [52] F. Hanif, D. Das, J. Halliwell, D. Home, A. Mazumdar, H. Ulbricht, and S. Bose, (2023), [arXiv:2307.08133 \[gr-qc\]](#).
- [53] M. A. Lohe, **Journal of Physics A: Mathematical and Theoretical** **42**, 035307 (2008).
- [54] E. Pinney, **Proceedings of the American Mathematical Society** **1**, 681 (1950).
- [55] H. R. Lewis, **Phys. Rev. Lett.** **18**, 510 (1967).
- [56] H. R. Lewis, **Journal of Mathematical Physics** **9**, 1976 (1968), <https://doi.org/10.1063/1.1664532>.
- [57] G. Mahajan and T. Padmanabhan, **General Relativity and Gravitation** **40**, 661 (2008).
- [58] K. Rajeev, S. Chakraborty, and T. Padmanabhan, **General Relativity and Gravitation** **50**, 116 (2018).
- [59] R. Simon, E. C. G. Sudarshan, and N. Mukunda, **Phys. Rev. A** **36**, 3868 (1987).
- [60] R. Simon, E. Sudarshan, and N. Mukunda, **Physics Letters A** **124**, 223 (1987).
- [61] W. B. Case, **American Journal of Physics** **76**, 937 (2008), https://pubs.aip.org/aapt/ajp/article-pdf/76/10/937/13118327/937_1_online.pdf.
- [62] M. Morikawa, **Phys. Rev. D** **42**, 2929 (1990).
- [63] N. Ripamonti, **Journal of Physics A: Mathematical and General** **29**, 5137 (1996).
- [64] S. L. Braunstein and P. van Loock, **Rev. Mod. Phys.** **77**, 513 (2005).
- [65] U. Leonhardt and H. Paul, **Progress in Quantum Electronics** **19**, 89 (1995).
- [66] S. Ghosh, K. S. Gupta, and S. C. L. Srivastava, **EPL (Europhysics Letters)** **120**, 50005 (2017).
- [67] L. Hackl, E. Bianchi, R. Modak, and M. Rigol, **Phys. Rev. A** **97**, 032321 (2018).

- [68] K. Lochan, K. Parattu, and T. Padmanabhan, *General Relativity and Gravitation* **47**, 1841 (2014).
- [69] K. Andrzejewski, *Quantum Information Processing* **21**, 117 (2022).
- [70] A. Serafini, F. Illuminati, and S. D. Siena, *Journal of Physics B: Atomic, Molecular and Optical Physics* **37**, L21 (2003).
- [71] G. Adesso, D. Girolami, and A. Serafini, *Phys. Rev. Lett.* **109**, 190502 (2012).
- [72] J. Grain and V. Vennin, *Journal of Cosmology and Astroparticle Physics* **2020**, 022 (2020).
- [73] J. Campbell, *J. Phys. A.* **42**, 365212 (2009).
- [74] I. A. Pedrosa, *Journal of Mathematical Physics* **28**, 2662 (1987), https://pubs.aip.org/aip/jmp/article-pdf/28/11/2662/8156300/2662_1_online.pdf.
- [75] V. F. Mukhanov, H. A. Feldman, and R. H. Brandenberger, *Phys. Rept.* **215**, 203 (1992).
- [76] A. R. Willms, *SIAM Journal on Matrix Analysis and Applications* **30**, 639 (2008), <https://doi.org/10.1137/070695411>.
- [77] P. Jain, S. M. Chandran, and S. Shankaranarayanan, *Phys. Rev. D* **103**, 125008 (2021).
- [78] S. Choudhury, R. M. Gharat, S. Mandal, and N. Pandey, *Symmetry* **15** (2023), 10.3390/sym15030655.
- [79] N. D. Birrell and P. C. W. Davies, *Quantum Fields in Curved Space*, Cambridge Monographs on Mathematical Physics (Cambridge University Press, 1982).
- [80] P. Caldirola, *Il Nuovo Cimento (1924-1942)* **18**, 393 (1941).
- [81] E. Kanai, *Progress of Theoretical Physics* **3**, 440 (1948), <https://academic.oup.com/ptp/article-pdf/3/4/440/5250274/3-4-440.pdf>.
- [82] E. Bianchi, L. Hackl, and N. Yokomizo, *Journal of High Energy Physics* **2018**, 25 (2018).
- [83] K. Boutivas, G. Pastras, and N. Tetradis, *Journal of High Energy Physics* **2023**, 199 (2023).
- [84] D. Katsinis, G. Pastras, and N. Tetradis, (2023), [arXiv:2304.04241](https://arxiv.org/abs/2304.04241) [hep-th].
- [85] E. Bianchi, L. Hackl, M. Kieburg, M. Rigol, and L. Vidmar, *PRX Quantum* **3**, 030201 (2022), [arXiv:2112.06959](https://arxiv.org/abs/2112.06959) [quant-ph].
- [86] R. N. Raveendran and S. Chakraborty, (2023), [arXiv:2302.02584](https://arxiv.org/abs/2302.02584) [astro-ph.CO].
- [87] M. Ahmadi, S. Das, and S. Shankaranarayanan, *Can. J. Phys.* **84**, 493 (2006), [arXiv:hep-th/0507228](https://arxiv.org/abs/hep-th/0507228).